SKYLAB EXPERIMENT M552
EXOTHERMIC BRAZING

By

J. R. Williams
Process Engineering Laboratory
Marshall Space Flight Center
Alabama 35812

SUMMARY

The M552 Skylab experiment reveals that brazing in space is feasible. It successfully demonstrated the ability to retain molten metal within a braze tube joint system. Surface energy was the dominant operative force system controlling liquid metal for this experiment.

The zero gravity environment for brazing resulted in several differences; increased solubility, increased liquid spreading, more uniform menisci (liquid/vapor interface) and a reduction of braze alloy shrinkage defects. The residual radioactive intensity and location of the redistributed isotope was interpreted to provide a sequential history of braze alloy movement during the-melt-flow-solidification stages of the process.

Convection theory [4] applied to M552 was validated but some results were not explainable by it, i.e., increased nickel transport and the radial mixing of the silver isotope on samples SLN-2 and SLN-4. All characteristics of thermal analysis appeared to react as expected but heat conduction rates increased because of increased extent, rate and uniformity of braze alloy spreading [5].

INTRODUCTION

The objectives of this experiment were to evaluate brazing as a tube joining technique for the assembly and repair of hardware in space and to study the spreading, mixing and capillary action of molten braze material in near zero gravity.

Experiment Results presented by C. M. Adams - University of Wisconsin.

The Exothermic Brazing Experiment was proposed late in 1965 as the MSFC # 35 experiment for the Saturn IV-B Workshop, and in September 1966, it was approved as Experiment M492, Tube Joining in Space. The initiation of the proposal was motivated by Air Force programs with exothermic heating sources which could be operated at pressures as low as 10^{-6} Torr. In the ensuing years, under contracts with the Whittaker Corporation, exothermic material compositions and configurations were developed for the M492 experiment and verified by extensive testing at MSFC.

In 1968, the M492 experiment was re-evaluated and approved by NASA as the Exothermic Brazing task of the M512 series of experiments. Later the experiment number and name were changed to the M552 Exothermic Brazing Experiment. Qualification and hardware testing continued through 1972, preparing the experiment for the 1973 Skylab flight. On June 12 and 13, 1973, Astronaut Paul J. Weitz processed four (4) braze specimens on NASA's earth orbiting Skylab.

The following organizations assisted NASA in the design, testing and analyses of the experiment: Battelle Columbus Laboratories - Metallographic Analyses; Lockheed Missiles and Space Company - Solidification and Connection Theory; Massachusetts Institute of Technology - Thermal Analyses; Union Carbide Corporation (Oak Ridge National Laboratory) - Isotope Tracer Application; University of Wisconsin - Metallographic Analyses; Westinghouse Astronuclear Laboratory - Surface Tension and Adhesion Analyses; Whittaker Corporation - Exothermic Material Development; Hayes International - Test Operations and the Naval Research Laboratory - Experiment Consultation. To the personnel representing these organizations and many NASA personnel, the author wishes to express sincere thanks for their professional guidance and dedication to this historic and successful engineering endeavor.

HARDWARE DESCRIPTION

EXOTHERMIC BRAZING ASSEMBLY

Each of the four braze specimens consisted of a tube, sleeve, inserts (spacers), and silver-copper-lithium braze rings. Each specimen, possessing a different clearance gap between the tube and sleeve, was positioned in a separate canister containing the exothermic material, ignitors and insulation. This assembly is shown in Figure 1. Two of the four specimens contained pure nickel tubes and sleeves. An isotope, 110-Silver with a half life of 253 days, was added to a section of one braze ring in the nickel specimens to enhance analysis of capillary flow. The location of the isotope pellet prior to melting is shown in Figure 2. The other two tubes and sleeves were

type 304L stainless steel with the tube partially slit through the center cross section but with some solid portions for support and to simulate a butt joint. Sample identification, material and gap clearances between the sleeves and tubes are noted in Table I.

BRAZE ALLOY RINGS

Each braze alloy ring weighs 1.95 grams and was composed of 71.8 percent silver, 28.0 percent copper, and 0.2 - 0.4 percent lithium. The alloy's melting temperature was 760°C (1410°F).

EXOTHERM MATERIAL

Three exotherm rings with a combined weight of sixty grams were installed over the sleeve to provide the heat source required to produce a brazed tube and sleeve joint. Substantially all of the reaction products were solid, and no external oxygen supply was required for the reaction. The exotherm material ignites at 1104°C (2020°F) and produces 650 calories per gram. Approximately 90 seconds are required for the exotherm to complete its reaction. The exotherm used in the M552 experiment has the following composition:

Aluminum	24.8 percent
Boron	5.0 percent
Titanium Dioxide	55.2 percent
Vanadium Pentoxide	15.0 percent

IGNITORS

Two ignitors positioned against the exotherm ring, were used to initiate the exotherm reaction. Although one ignitor is normally sufficient, the second one was added to provide redundancy to the system. This ignitor exotherm material reacts at 510°C (950°F) and has the following composition:

Aluminum	14.8 percent
Boron	7.7 percent
Titanium	10.0 percent
Vanadium Pentoxide	67.5 percent

INSULATION

The exothermic material was surrounded with Fiberflax (fibrous aluminum oxide) insulating material which contained the heat generated for the brazing process and also protected the outside container from overheating.

HOUSING

The aluminum housing which held the four exothermic brazing packages was made in two halves, and after installation of four exothermic packages, was bolted together on the line shown along its median plane. See Figure 3. A thermocouple temperature sensor was bolted onto the top half portion of the housing, and electrical connections to this sensor and to the ignitor wires in the exothermic packages were soldered to an insulated terminal board attached to the top half of the housing. All electrical connections were led out of the case through the power connector on the cover. Figure 4 shows a photograph of the total exothermic assembly during final assembly of all major components including the brazing packages and the terminal board.

ELECTRICAL - TEMPERATURE CHARACTERISTICS

Power for initiation of the exothermic reactions was provided by the 28 vdc batteries contained in the M512 facility and controlled through selector and trigger switches on the facility's control panel within the Skylab's Multiple Docking Adaptor. Each initiating pulse is 120 amperes at 28 volts for 5 milliseconds (14.4 watt seconds per pulse). The temperature sensor output on the M512 chamber was read on the control panel's temperature gauge. The thermocouple sensor closes a circuit at approximately 110^{o}F and this action was displayed by a hot light indicator on the control panel. A schematic diagram of the experiment's electrical system is shown in Figure 5.

EXOTHERMIC PACKAGE WEIGHT AND SIZE

Equipment Item	Weight	Volume	Dimensions
Exothermic Brazing Assembly	3.7 Kg (8.2 lbs)	387 in^3	6.75" x 7.61" x 7.56"
Power Cable	.23 Kg (.5 lbs)	1.00 in^3	3/8" dia x 12"

A picture of the complete M552 Exothermic Brazing Package with its electrical power cable is shown in Figure 6.

PROCEDURES

PREFLIGHT DEVELOPMENT

During the development of the Exothermic Brazing Experiment, tests were performed at MSFC and at contractor facilities on over sixty prototype brazing packages similar to the four which were processed in the Skylab experiment. This testing included subjecting the units to relative humidity, vibration, exotherm aging, oxygen rich atmospheres and temperature profile tests under a simulated space experiment condition within the M512 experiment processing facility similar to that used in the Skylab flight experiment. A cataloging of the brazed specimens used in the qualification and evaluation phase of the experiment is shown on Table I.

These tests provided the base line data for the operational procedure of M552 Exothermic Braze Experiment in Skylab. Three M552 Exothermic Braze experiment assemblies (4 exothermic packages in each assembly - 12 packages total) similar to the flight configuration were used for astronaut training at JSC at Houston, Texas.

In addition, two nickel material specimens with a radioactive tracer, 110-Silver, were brazed for the Oak Ridge National Laboratory personnel who developed the isotope mapping techniques subsequently applied to the Skylab specimens. Testing was also performed to assure the safety of Skylab crew and photographic film relative to the radiation effect of the isotopes. Three specimens were brazed at MIT from which a thermal analysis for the experiment was derived. A temperature profile graph of the heat transferred to the tube's inside diameter is shown on Figure 7. Thermocouple locations for this test are shown on Figure 8.

Twelve other specimens of flight configuration were brazed at MSFC prior to the flight experiment. A typical laboratory test setup is shown in Figure 9. These brazed specimens served as radiographic and metallographic references for comparison with the specimens brazed during the Skylab flight which were jointly analyzed by the MSFC and experiment consultant personnel. One Exothermic Brazing Experiment assembly containing four tube and sleeve assemblies was reserved as a backup flight package or to be used for tests to duplicate any unexpected conditions encountered during the flight experiment.

As a result of the above engineering studies, confidence in the adequacy of the operational hardware and astronaut procedures was established.

FLIGHT PROCEDURE

Astronaut Weitz installed the M552 package in the M512 processing chamber in the Skylab MDA. The chamber door was sealed and the chamber atmosphere vented to space. After a 2 hour outgassing period, he initiated the ignition process. Approximately 2.75 hours was required for one exothermic package to be processed through its temperature profile. The other 3 units were processed similarly. All hardware and facility systems worked as designed; no anomalies were observed. The experiment package containing processed exothermic units was returned to earth on June 22 and to MSFC on June 26, 1973.

POST FLIGHT EVALUATION

The M552 package was received at MSFC and sequentially photographed during unpackaging. Visual observations were made and recorded. All four canister assemblies were x-rayed. The individual Skylab specimens, SLS-1, SLN-2, SLS-3 and SLN-4 were removed and cleaned via wire brush. Montage x-ray pictures were made of each specimen. Autoradiographs were made of the two nickel specimens. The negatives were printed and are shown on Figures 10 and 11. The 2 nickel specimens, SLN-2 and SLN-4, were transferred to Oak Ridge National Laboratory for sectioning and isotope mapping. The two 304L specimens were transferred to Battelle for sectioning. The identification plan for sectioned samples is shown on Figure 12.

Battelle subsequently provided the metallographic evaluation of both narrow gap samples SLS-1 and SLN-2. The University of Wisconsin provided the metallographic evaluation of the wide gap samples SLS-3 and SLN-4. A total matrix showing disposition, allocation, etc., of all preflight characterization and flight samples is shown on Table I.

FUTURE WORK

NASA Contract NAS8-28733, with the University of Wisconsin has been extended to study why certain liquid-solid reactions, such as the dissolution of nickel takes place more rapidly in the space environment. This effort will run through calendar year 1975.

RESULTS AND DISCUSSION

RADIOGRAPHY

I. SLS-1 (GAP .005" - 304L Material) specimen montage X-ray is shown in Figure 13 and is compared with a typical ground brazed sample MCS-1 of the same configuration. The Skylab sample exhibited a nearly perfect braze joint. One minor shrinkage defect was present adjacent to a ring groove at station F. Excess braze alloy had flowed inwardly through the slits in the tube and pooled over and adjacent to these slits on the tube I.D. The braze material was free from oxide. The braze alloy completely spread to the outermost ends of the sleeve. MCS-1 was typical of the ground brazed .005" GAP characterization samples, all of which exhibited voids adjacent to ring grooves and a much higher frequency of small defects throughout the solidified braze zone. It should also be noted that a .005" GAP exceed normal design specification for braze joint in one gravity application. A normal design clearance for optimum capillary braze flow in one-gravity would be approximately .002".

II. SLN-2 (GAP .010" - Nickel Material) specimen montage X-ray is shown on Figure 14 and is compared with a typical ground brazed sample MCN-1 of the same configuration. In this specimen the gap volume basically equals the volume of braze alloy. All specimens, Skylab and ground retained some braze metal in the ring groove. This would indicate equalizing forces between the ring groove to retain the molten metal and the gap zone to draw the metal into it. Both Skylab and Ground samples exhibited void areas in the braze gap zone.

III. SLS-3 (GAP .020" - 304L Material) specimen montage is shown in Figure 15 and is compared with a typical ground brazed sample of the same configuration. This specimeb was designed to represent a starved braze joint, possessing only about 50% enough alloy to fill the .020 gap zone. Note in the ground sample MCS-4, brazed horizontal, all the braze metal had pooled at the bottom section and gravity forces had completely drained the ring grooves. The Skylab sample is a classic example of what happens when surface energy is the dominate force. A small quantity of braze alloy was retained as fillets in both ring grooves and most braze alloy had bridged the .020 gap between the tube and sleeve. Some braze alloy was drawn through the 3 slits and pooled internal on the tube.

On the SLS-3 the braze material is free from porosity and voids. It is logical to assume that the .020" gap would have completely filled had there been adequate braze alloy.

IV. SLN-4 (GAP .000" - .030" - Nickel Material) specimen montage X-ray is shown in Figure 16 and is compared with a typical brazed sample MCN-4. The braze quality of the Skylab specimen was very good and much better than any ground brazed characterization sample. Note that nearly all of the braze alloy was drawn from the SLN-4 ring groove at the left side of the photograph and at the narrow end of the gap. Braze alloy fillets on both ground and flight specimens were retained in the ring groove adjacent to the wide gap end. Variation in the contour lines of the braze alloy were caused by slight variations in concentricity between the sleeve and tube. Radioactive tracings indicate alloy spreading the full length of the sleeve and some fillets of alloy were visible adjacent to the inserts at the wide end of the gap.

ISOTOPE - 110 SILVER TRACER APPLICATION [3]

I. AUTORADIOGRAPHS

Autoradiographs which were made from both samples SLN-2 and SLN-4 are shown in Figure 10. In these autoradiographs the darker areas correspond to higher levels of radioactivity. The 360° azimuth represents the circumference of the nickel sleeve, and the original position of the tracer-containing pellet is marked on the print. The autoradiograph for sample SLN-2 shows that the tracer alloy flowed mainly in a circumferential direction to areas at an azimuth of about 180° from the original tracer pellet location (0°). Most of the radioactivity is located in proximity to the pellet ring groove. An area of low radioactivity content can be seen just inside the tracer pellet location near the "upper" braze ring groove. After brazing in zero gravity, the tracer alloy in sample SLN-4 appeared to be concentrated in two areas; one above and the other below the tracer pellet location, although there was some mixing of the isotope throughout the total taper gap braze zone. This is shown in Figure 11.

II. ISOTOPE INTENSITY MAPS

The first use of a radioisotope tracer for mapping flow patterns during brazing of metal components in a space environment (near zero gravity) proved successful.

Radioisotope tracing consisted of measuring the intensity of radiation from the silver isotope at numerous points around the braze filled annulus at many transverse sections of the tube. Individual radiation intensity results for all sections were then combined to generate a two-dimensional radiation intensity map of the entire braze joint. These maps are shown in Figure 17 for SLN-2 and Figure 18 for SLN-4.

In both unit and near-zero gravity experiments, flow of braze material into "hot zones", generated by uneven ignition of the exotherm during the initial stages of the braze, was evident. This phenomenon would not have been observed without the use of the radioisotope tracer-containing alloy.

It is interesting to note that the areas void of solid braze alloy, yet wet by molten braze material, showed no residual tracer isotope activity. This observation would imply that the silver did not react nor adhere to the nickel surface.

The ^{110}Ag tracer maps for this experiment suggest that such tracing can provide a picture of the thermal history for any particular assembly as well as accurate braze alloy flow information. Since no other analytical technique would provide this unique composite view of surface, gravitational, and thermal forces, radioisotope tracing proved useful in interpreting other metallurgical aspects of this experiment.

SLN-2. The radiation intensity map for sample SLN-2 is shown in Figure 18. This sample had a nominal annulus clearance of 0.010 in. (0.025 cm). Some of the braze alloy flowed outside the nickel ferrule in the samples brazed in space. The effect of this extraneous flow is also shown by the movement of the tracer alloy which extended outside

the zero reference plane to areas with negative distance values. However, most of the tracer alloy was concentrated on either side of the ring groove from an azimuth of approximately 40°, moving to the left to 200°. An area of slight activity was found in the "upper" ring groove associated with a fillet of braze material. These results agree with those observed in the autoradiograph for sample SLN-2 showing high radioisotope content along the "lower" ring groove.

SLN-4. The radiation intensity map for sample SLN-4, having a 0.000-0.030 in. (0.000-0.076 cm) taper annulus, is shown in Figure 18. The braze extended beyond the nickel ferrule, and moderate concentrations of the radioisotope were detected outside the ferrule edge at negative distance values. However, most of the ^{110}Ag tracer isotope was concentrated in areas above and below the tracer ring groove at an azimuth of approximately 280 . Since SLN-4 was a taper-gap sample, it must again be remembered that the lower concentration area inside the ring groove actually gave higher radiation intensity values than the high concentration area outside the groove, but these latter values were normalized by dividing by a smaller volume increment. With this normalization in mind, comparison of the tracer map in Figure 18 to the autoradiograph in Figure 11 can be made. Both the map and autoradiograph show the presence of two regions of intense radioactivity, and they agree with respect to their azimuthal location.

CONVECTION ANALYSIS [1 & 4]

Specific evaluations performed for this experiment include:

Examination of the extent and uniformity of spreading using data supplied by other investigators.

Evaluation of the location of voids taking into account solidification shrinkage, buoyancy, Marangoni effect and the presence of the tube slot.

Analysis of the microstructure data obtained by others especially near the free surface where surface tension convection might occur even in low gravity.

Based on results reported to date, the following low-gravity variations have been observed.

I. Spreading of braze alloy: Visual and metallurgical examinations indicate the molten braze alloy spread further and more uniformly in the constant gap Skylab samples, SLS-1, SLN-2 and SLS-3, than in the corresponding ground samples [7 and 8]. A superior quality braze joint was noted in the SLS-1 sample [7]. Thus, the predictions of improved capillary flow [4] were confirmed. No firm conclusion can yet be reached on the absence or presence of turbulence during capillary spreading in microgravity. Turbulence was only expected to be possible in Skylab specimens SLS-3 and SLN-4.

II. Lack of hydrostatic pressure: A more symmetrical interface was noted in the meniscus of Skylab sample SLN-2. Spreading was more extensive in wide gap Skylab specimens SLS-3 and SLN-4 than in the corresponding ground samples [8]. These low-g variations agree with predictions dealing with the lack of hydrostatic pressure in microgravity brazing.

III. Void location: In Skylab sample SLS-1 there was an absence of voids and porosity compared to ground specimens. This low-g variation could be attributed to the more uniform capillary spreading in microgravity. In Skylab sample SLN-4 porosity existed near the narrowest position of the gap which was not seen on ground based tests MCN-4, -5 and -6. This porosity has been attributed to solidification shrinkage, thus Marangoni bubble migration cannot be a factor. From thermal conduction considerations the axial ends should solidify before the center and the igniter end should solidify before the opposite end. Thus, porosity should be centered between the middle section of the braze alloy and the end opposite the igniter. The wide gap ground samples, however, would be influenced by thermal convection, as well

thermal conduction, and the last portion to solidify in these vertically processed specimens would have been the wide gap (upper) end. Thus, ground specimens MCN-4, -5 and -6 would be expected to have less shrinkage induced voids near the narrow gap end than SLN-4, as actually occurred.

IV. Distribution of components: Two significant low-g variations have been reported thus far: (1) increased nickel transport in the SLN-4 wide gap, and (2) complete radial mixing of the silver isotope in SLN-2 and SLN-4. Nickel distribution was greater in the wide gap samples MLN-4, -5 and -6 [7]. This increased nickel transport cannot be attributed to surface tension convection because $\sigma_{Ni} > \sigma_{Ag-Cu}$. Furthermore, this mechanism, if possible, would have been operative on Earth also. Neither can gravity convection explain the increased Skylab nickel transport because $\rho_{Ni} \simeq \rho_{Cu} < \rho_{Ag}$. This would cause nickel to rise to the wide gap area in ground samples MLN-4, -5 and -6. The preceeding argument assumes that nickel is completely miscible in molten Ag-Cu. The phase diagram of Ag-Ni however, indicates a monotectic system with the possibility of two immiscible liquid phases if melt temperatures exceed 1435°C [9]. The silver-rich liquid is approximately 1.5 wt % Ni and the nickel-rich liquid is 3.65 wt % Ag. At the monotectic temperature the various molten components have the following densities:

Melt Component	Density at 1435°C (g/cc)
Copper	7.69
Ni-rich	7.81
Ag-rich	8.87

Thus, the narrow gap in samples MLN-4, -5 and -6 would be depleted in nickel, and again gravity convection would not explain the increased nickel in the wide gap of SLN-4. In conclusion the low-g variation of increased nickel transfer in SLN-4's wide gap cannot be explained by surface tension or gravity effects and must therefore be due to some as yet unexplained phenomenon such as nucleation or solidification effects. It should also be pointed out that no quantitative information has been reported on M552 alloy distributions, only qualitative results.

ρ - Density
σ - Surface Tension - Stefan - Boltzmann Constant

Silver isotope tended to settle (Ag is densest component) in ground samples MCN-1, -2, -3, -4, -5 and -6; whereas complete radial mixing of the isotope was reported in Skylab samples SLN-2 and SLN-4 [7]. As predicted in Section III-B, the ground based settling is due to gravity-induced sedimentation. The unexpected complete radial mixing which occurred on Skylab can be attributed to liquid-state diffusion and/or turbulence in the capillary flow.

V. Transport: The subject of transport and distribution of components was also addressed by R. W. Heine, C. M. Adams and T. A. Siewert [1]. These investigators offer the following comments:

Both Skylab nickel specimens (the one examined at Battelle and the other at the University of Wisconsin) exhibited appreciably higher concentrations of dissolved nickel in the braze alloy than did any of the ground characterization specimens. Several explanations, most of them unreasonable, may be hypothesized. It seems very unlikely that the absence of gravity would materially influence either the solubility or the diffusivity of nickel in a silver-rich liquid. In fact, the combinations of time, temperature, and liquid state diffusivity, and the dimensions of the capillary space in the nickel specimens, are such that diffusion cannot be the limiting factor. Even with the wide (0.020 inch) gap nickel specimen, the time, t, required for nearly complete diffusion throughout the capillary section can be estimated from

$$t = \frac{0.2L^2}{D}$$

where $L = 0.020" = 0.051$ cm., gap clearance

$D = 2.8 \times (10)^{-5} \text{cm}^2/\text{sec}$ (2, 3), diffusivity in liquid silver at 1000°C

$t = 18$ seconds

This specimen is obviously at elevated temperature much longer than 18 seconds. If diffusion is augmented by convection, the time becomes even less. However, the transport situation is evidently complicated

enough that it has not yet proven possible to establish a good analytical representation. It does seem that convection has an effect on transport at the interface between the solid nickel and the braze alloy. In both the ground characterization and Skylab specimens, there develops a layer of copper-nickel alloy at this interface. In the absence of convection, this layer develops sufficient thickness to act as an effective diffusion barrier. Weighing all the facts and observations, it seems likely convection was more vigorous in the Skylab than in the ground characterization specimens. The interface structure reflects this; there is a distinct tendency for the copper nickel interface layer to be thinner in the Skylab than in the ground characterization specimens. This is not uniformly true, in fact, the observation must be and has been made statistically by close scrutiny of many portions of the interface on each specimen.

In summary, the present conclusion is there was sustained convection after capillary flow in the Skylab specimens which was sufficiently vigorous to prevent development of an effective copper-nickel alloy diffusion barrier. It is postulated this sustained convection may have resulted from the interaction of the traveling Skylab specimens with the earth's magnetic field.

VI. Braze-base metal reaction: Nucleation of nickel phases in the nickel samples, both ground and Skylab, should vary with gap width [4]. This effect has been tentatively identified in SLN-2 [10] along with a possible gravity effect on this phenomenon. While the cause of this effect (surface energy considerations) should not vary with gravity, nickel transport variations due to gravity may have led to reported gravity variations in nickel-braze structure as well as reported gap size variations. The orientation of the nickel rich solid phase also seems to match the theories discussed in [4] as the nickel-rich needles are perpendicular to the walls [10].

VII. Microstructure: Different and/or unique microstructures were reported in Skylab samples SLN-2, SLS-4 and SLN-4. These low-g variations in microstructure are:

A. SLN-2: A unique structure appeared in which a globular copper-nickel second phase is in a matrix silver phase with the globular phase present at between 30 and 90 volume percent. Also, a unique structure appeared in which a needle-like second phase, high in copper, is present in a silver matrix phase. The needles are perpendicular to the joint interface.

B. SLS-3: The proeutectic silver-rich phase was more noticeable than in the ground samples and SLN-4 specimen.

C. SLN-4: Altered copper structure in the narrow gap end when compared to ground samples. Presence of proeutectic silver-rich phase not found in ground samples.

Based on the qualitative nature of these results, these variations have been attributed to some unknown nucleation effects and not to convection effects.

VIII. Variable-gap capillary pumping: As expected [4] the melt in both the Skylab and ground-based variable gap samples SLN-4, MCN-4, -5 and -6 moved to the narrow end of the tube. No low-g variation was expected because capillary forces predominate in this configuration.

III. METALLURGICAL STUDIES [1 & 6]

A. PHASE RELATIONSHIPS

The pertinent binary equilibrium systems, copper-nickel, silver-copper, and silver-nickel, are well established, but the ternary system, silver-copper-nickel, is not known with precision. Copper and nickel are mutually completely soluble in both the liquid and solid states; silver and copper exhibit complete liquid but limited solid solubility; silver and nickel exhibit very limited mutual solubility in both the liquid and solid states. The one published study of the ternary system suggests that silver-copper alloys rich in silver exhibit very limited capacity for dissolving nickel except at very high temperature [11]. Alloy element distributions observed in both the Skylab and ground characterization specimens exhibit appreciable concentrations of nickel in the solidified braze alloy. Moreover, much more nickel dissolved in the Skylab specimens than in the ground-based specimens.

The binary silver-copper alloy without nickel separates upon solidification into two solid phases, one rich in copper but containing some dissolved copper. When nickel is added to the silver-copper alloy, upon solidification the nickel preferentially associates with the copper-rich phase, being quite insoluble in the silver-rich phase. Moreover, silver and nickel appear to be mutually exclusive in the copper-rich phase. In fact, two kinds of copper-rich phase form, one which contains nickel but no silver, and the other which contains silver but almost no nickel. The solidification process is rendered quite complicated by the addition of nickel. The simple binary 72% silver 28% copper freezes substantially at one temperature, 780°C, and the product of solidification exhibits the classical eutectic structure, a finely dispersed mechanical mixture of silver-rich and copper-rich phases. The presence of nickel increases the temperature at which solidification begins, and the first solid crystals which form contain copper and nickel with practically no silver. These crystals become fairly large before the rest of the alloy freezes at about 780°C. These large copper-nickel crystals or dendrites are called primary because they form first upon cooling. Both the ground characterization and Skylab specimens of brazed nickel exhibited this characteristic strucfeature. Some primary copper-rich dendrites were also observed in the stainless steel specimens, but these contained much less nickel, because stainless only contains 8% nickel. As more and more nickel dissolves in

the silver-copper alloy, the fine eutectic structure progressively, and finally completely, disappears. Very abnormal structures, surprisingly high in nickel concentration, were observed only in the Skylab samples. The identification of these abnormal structures with high nickel concentration is still somewhat circumstantial; the important question is: Is the structure abnormal because of the absence of gravity, or is the structure abnormal because so much nickel has dissolved? And further, did more nickel dissolve because of the absence of gravity? At this stage of the study it appears that the increased nickel concentration in the Skylab specimens accounts for the abnormal structure.

The presence of dissolved nickel in the liquid silver-copper alloy has a subtle but logical effect on the formation of primary phases. In the absence of nickel, solidification of the 72% silver 28% copper substantially begins and ends at 780°C, and the structure produced is a finely dispersed classical eutectic mixture of silver-rich and copper-rich phases. The first effect of dissolved nickel is to increase the temperature at which solidification begins: A copper-rich primary phase, containing nickel, forms at a temperature well above 780°C. Upon cooling, when the temperature begins to approach 780°C; virtually all the nickel has been rejected from the liquid solution, because the nickel is virtually insoluble in the silver-rich liquid at temperatures below 850°C. Thus, it is the nickel which causes the primary copper phase to form at a relatively high temperature; however, this primary crystallization has the effect of removing copper from the liquid. The remaining liquid contains appreciably more than 72% silver, and primary silver-rich phase now must form at a temperature about 780°C. When the eutectic temperature, 780°C, is finally reached, whatever liquid still remains contains very nearly 72% silver-28% copper, and freezes to a fine eutectic structure. If the initial nickel concentration in the liquid is high enough, solidification will become nearly complete at a temperature above 780°C, and no normal eutectic structure will form. "The two-phase field resulting from the silver-copper eutectic decomposition terminates with the addition of 5 wt % Ni."[12] The quotation is an interpretation of early work done on the silver-copper-nickel ternary system[11], and is qualitatively correct. The limiting value of 5% nickel, in light of the present study, appears to be somewhat low; the actual value is probably closer to 10% nickel.

B. STRUCTURE AND COMPOSITION

(1) Wide Gap Specimens

The findings reported in the following paragraphs evolved primarily from brazed stainless steel samples SLS-3, and MCS-4,-5, and -6, and brazed Ni samples SLN-4 and MCN-4,-5, and-6. These have been referred to as "wide gap" samples, because, to develop effective capillary flow on earth using these materials, gap clearances are generally held below 0.005 inch. One objective which influenced specimen design was to observe wide-gap capillary flow in the absence of gravity.

(2) Nickel Specimens

In Figures 19, 20 and 21 are shown photomicrographs of structures found within the capillary brazed joint in specimen SLN 4. These structures are normal in most respects, being almost identical to corresponding sections taken from the ground characterization sample, Figure 22. The fine eutectic mechanical mixture occupies most of the field of view. The large dark regions are copper-rich and contain some nickel but almost no silver. The small dark regions are copper-rich and contain some silver but very little nickel. The white regions are silver-rich, containing some copper but essentially no nickel. In the Skylab specimens there occasionally appears a relatively large primary silver-rich dendrite; this has never been observed in any of the ground characterization specimens, and is an indirect result of high nickel concentration.

The alloy element distribution is typified in Figures 23, 24 and 25 which are, respectively, electron microprobe area scans showing nickel, copper, and silver distributions in the same field of view shown in Figure 22. In particular, it can be seen the large copper-rich dendrites contain copper and nickel but essentially no silver, and the small dark areas (sometimes referred to as secondary copper-rich phase) are rich in copper but contain no nickel. This pattern of alloy element distribution is repeated throughout in both the Skylab and ground characterization specimens, and supports the statement made above that silver and nickel are substantially mutually exclusive in the copper-rich phase, a feature which complicates the solidification sequence. Measurements were made of a structural feature called dendrite arm spacing. In the tree-like growth of dendrites, there occur regions in which the arms of the dendrites are

quite regularly spaced, and it has been found this spacing depends systematically on alloy composition and the cooling rate which prevailed during solidification. Dendrite arm spacings were found to be the same in the Skylab as in the ground characterization specimens, as had been expected. A typical view permitting measurement of dendrite arm spacing is shown in Figure 26, where the spacing is consistent with a dendrite containing 10% nickel 90% copper which solidified at a cooling rate of about 50°C per minute [13].

The structures observed in the nickel Skylab specimens have been characterized as normal, abnormal and mixed. These structures are shown in Figures 27 through 30. Figure 27 from Skylab sample SLN 4 shows the normal structure, which is to say it is substantially identical in all important features to the brazed nickel ground characterization specimens. There are occasional large nickel-containing copper-rich, silver-free dendrites to be found throughout the braze alloy. Then, near the interface, there are peninsular protuberances, epitaxial with the solid nickel, which are also rich in copper with appreciable concentrations of dissolved nickel. The rest of the structure is the fine eutectic mixture of silver-rich (white) solid solution containing relatively small particles of copper-rich, silver-bearing, low nickel solid solution. A detailed microprobe survey of this structure gave the following results?

a. Near the center of a large dendrite the composition is 20% nickel 80% copper.

b. Near one of the tips of the same large dendrite the composition is 10% nickel 90% copper.

This alloy distribution is consistent with the nature of dendrite growth. The first material to form upon cooling has the highest nickel content, and then, as the crystal grows, the exterior regions exhibit progressively lower nickel concentrations, and form at progressively lower temperatures. This is often referred to as a cored structure. The proturbances growing from the brazed nickel interface also present a logical variation in composition.

c. In the protuberance, very near the original interface, the composition is 35% nickel 65% copper.

d. Halfway out to the tip the composition is 20% nickel 80% copper.

e. At the tip the composition is 10% nickel 90% copper, the same as the tip of a large dendrite.

The small copper-rich particles within the finely dispersed eutectic structure contain something less than 10% nickel.

The abnormal structure is shown in Figure 28. There is a complete absence of the typically fine eutectic dispersion, and the relatively large dark particles contain nickel concentrations which range from about 40% nickel in their centers down to about 25% nickel near their exterior boundaries. These particles are therefore cored, but do not exhibit the usual morphology of dendrites. The total nickel concentration in the field of view shown in Figure 28 is quite high, estimated close to 10% nickel overall. Furthermore, the probe shows that the layer of nickel-copper alloy at the braze-nickel interface is quite thin compared to corresponding locations on ground characterization specimens. The thinner this layer the less effective it is as a diffusion barrier. Since it is unlikely any of these specimens reached temperatures much above 1000°C, the high nickel concentration is surprising in that it appears to exceed the maximum solubility which can be inferred from the published information on the ternary silver-copper-nickel system .

Figures 29 and 30 show mixed normal and abnormal structures. Figure 29 happens to be from a ring-groove location, where the cross-section of the braze alloy is relatively large, and Figure 30 shows a region within the capillary gap. All three structures, normal, abnormal and mixed, are found at various locations throughout the specimen; there is no systematic dependence on location.

(3) Stainless Specimens

Abnormal and mixed structures were not observed in any stainless

steel specimens, presumably because the stainless, containing only 8% nickel, does not introduce enough nickel into liquid solution to modffy eutectic solidification appreciably. Within the capillary gap in the stainless Skylab specimens, there is a pronounced tendency for primary silver-rich dendrites to form, clearly shown in Figures 31 and 32. In fact, in these regions there has been some impoverishment in copper, apparently by dissolution into the stainless; the copper is soluble in the solid stainless, whereas silver is not. However, primary silver-rich phase has never been observed in the ground characterization specimens. This is yet further evidence for enhanced transport in the Skylab specimens, which must, for reasons already stated, relate to convection, i.e. convective disturbance overcomes any tendency for an effective diffusion barrier to form at the liquid-solid interface. In the ring-groove of the stainless Skylab specimen, the structure is identical to that in the ground characterization specimens, exhibiting primary copper-rich dendrites, containing generally about 2% nickel (sometimes less), surrounded by normal finely dispersed eutectic structure (see Figure 33).

For comparison, structures observed in stainless ground characterization specimens are shown in Figures 34 and 35; these exhibit primary copper-rich phase together with normal eutectic. In the stainless Skylab specimen, primary silver-rich but no primary copper-rich phase is observed in the capillary gap, and primary copper-rich but no silver-rich phase was observed in the ring-groove location. In the nickel Skylab specimen, primary silver-rich and copper-rich phases were frequantly observed together (Figures 19 and 20), both primary phases resulting from the presence of nickel dissolved in the liquid prior to solidification.

Another curious feature of the stainless Skylab specimen was the presence of finely dispersed stainless steel particles within the braze alloy. The first inclination is to attribute these particles to the presence of debris remaining from machining the specimens. However, the specimens were very thoroughly cleaned, and the particles are extremely small, ranging from 0.5 to 5.0 microns (micrometers) in diameter. Stainless does not readily fragment into such fine particles; it is more likely these inclusions, shown in Figures 36 and 37 are the consequence of erosive attack of the stainless by the liquid metal. This is taken as still further evidence of vigorous convection peculiar to the Skylab specimens, because these

particles were not detected in any of the ground characterization specimens.

Summarizing, the results of examining the stainless steel Skylab and ground characterization specimens have revealed significant differences and similarities. The formation of primary copper-rich dendrites and normal fine eutectic structure was observed in all stainless specimens in the groove location. The stainless Skylab specimens was distinguished by the presence of primary silver-rich phase and non-uniform dispersion of very fine stainless steel particles within the braze alloy.

(4) Narrow Gap Specimens [6]

The findings reported in the following paragraphs evolved primarily from brazed stainless steel samples SLS 1 and MCS 1, 2 and 3 and brazed Ni samples SLN 2 and MCN 1, 2 and 3. All of these samples incorporated narrower capillary gaps approaching those normally used in conventional brazing.

(5) Nickel Specimens

The micro structure of the braze alloy in Skylab specimen SLN 2 was frequently different from the structure exhibited by ground based specimens as shown in Figure 38. The resulting micro structures clearly indicate variations in the braze alloy composition and perhaps some variation in the cooling rate. However, these micro structures are considered normal and there is no obvious relation to an effect of the micro gravity environment.

(6) Stainless Specimens

Skylab specimen SLS 1 was an essentially void free braze. The micro structure and many other characteristics is this braze were similar to comparable ground-based specimens. Also, as noted in the preceeding discussion of wide gap specimens, no abnormal or mixed structures were observed.

Both the nickel and stainless narrow gap specimens exhibited smaller braze alloy gaps than intended or observed in the ground-based specimens. The smaller gap probably resulted from an end restraint condition that prevented unrestricted thermal expansion of the assembly. In the case of the stainless specimen, a diffusion bond was formed in a tight gap region as shown in Figure 39. This observation confirms that diffusion bonding can also be used as a joining method in the micro gravity environment.

C. MENISCUS FORMATION

The retention of braze alloy in the corners of the oversize ring grooves and fillets formation in the Skylab specimens are significantly different from the ground brazed specimens. This observation clearly supports the enhancement of surface tension forces in a zero gravity field. This difference is shown in Figure 40 of Skylab samples SLS-1 and a 304L stainless sample brazed on the ground. A classic retained fillet is shown on Figure 41 of Skylab sample SLN-2 where complete fillet symmetry was obtained.

CONCLUSIONS

I. The absence of gravity greatly extends the scope of brazing and, thereby, the applicability of brazing to fabrication in space. In zero gravity environment, the surface tension forces driving capillary flow predominate, while on earth these forces must complete with gravity. Study of braze alloy distribution in Skylab specimens clearly indicates that dimensional tolerances, especially braze gap clearances, will be far less critical to joining operations in space than on earth. The .020" radial gap specimen was brazed; greater gaps could also be brazed. This, of course, could not happen in 1 g. The practical significance of this fact, which had been predicted but never tested, can hardly be overemphasized. In space fabrication, many joints, which on earth would be produced by welding, should probably be brazed to allow wider fit up tolerances.

II. The absence of gravity definitely and surprisingly changes the ways in which liquid and solid metals interact. For example, for the same time and temperature conditions of exposure (a) liquid silver-copper alloy dissolves nickel more rapidly in space than on earth, and (b) solid stainless steel dissolves copper from liquid silver-copper alloy more rapidly in space than on earth. The detailed mechanisms by which these reactions are hastened have not been positively identified, and this effect of space environment had not been predicted. The space environment appears to offer unique advantages for implementation of some liquid-solid reactions, and also the measurement of solubilities. For example, the Skylab experience clearly indicates a higher solubility of nickel in liquid silver-copper alloy than had been found in the earth-bound studies (in this reaction the silver is rejected and appears as almost pure metal); this is not because nickel is more soluble in space, but rather because it dissolves more rapidly. This pattern of behavior suggests that saturated liquid metal solutions can be more easily produced, and true solubilities are more easily determined in space than on earth.

III. Liquid-vapor boundary surfaces (menisci), and the flow of liquid metal driven by surface tension are in close conformance with what had been predicted for zero gravity environment. There were no unexplained effects and in the Skylab specimens the surface tension of liquid silver-copper alloy appears to have been quite uniform.

IV. The addition of a radioisotope tracer to the M552 brazing experiment provided a unique picture of the thermal history of braze melting within the annulus as well as useful representation of the braze alloy flow pattern during the melting solidification process. Silver isotope tended to settle (Ag is densest component) in ground samples; whereas complete circumferential mixing of the isotope was reported in Skylab samples. As predicted the ground based settling is due to gravity-induced sedimentation. The unexpected complete circumferential mixing which occurred on Skylab can be attributed to liquid-state diffusion and/or turbulence in the capillary flow.

V. The presence or absence of gravity has no observable effect on the mechanism of alloy solidification. Such microstructural details as dendritic configuration, and eutectic structure were the same in space as on earth.

VI. The Skylab specimens exhibited fewer and smaller shrinkage defects that the comparative ground processed characterization samples indicating that gravity forces are significant during the capillary movement of the braze alloy.

VII. The oxide build-up on both the M552 Skylab braze alloy and the substrate materials was less than on ground based specimens indicating the adequacy of utilizing the space vacuum and its infinete pumping capacity for brazing operations of this type configuration.

REFERENCES

1. Heine, R. W.; Adams, C. M.; Siewert, T. A.; Report on Flight/Ground Sample Comparison Relating to Flight Experiment M552, Exothermic Brazing, University of Wisconsin - Contract NAS8-28733, December 4, 1973.

2. Tobin, J. M.; Kossowsky, R.; Final Report on M551, M552 & M553. Research Study on Material Processing in Space - Contract NAS8-78730, Westinghouse Astronuclear Laboratory, Pittsburgh, Pennsylvania, December 12, 1973.

3. Braski, D. N.; Adair, H. L.; Kobisk, E.H.; Radioisotope Tracer Studies in the NASA Skylab Exothermic Brazing Experiment M552 - Contract No. W-74-5-ENG-26. Oak Ridge National Laboratory, Oak Ridge, Tennessee - (Operated by Union Carbide Corporation for the Atomic Energy Commission, December 1973.

4. Bourgeois, S. V., Convection Effects on Skylab Experiments M551, M552, M553 - Contract NAS8-28015, Lockheed Missiles & Space Company, Inc., Huntsville, Alabama, December 1, 1973.

5. Muraki, T.; Masubuchi, K.; Thermal Analysis of M551, M552, and M553 Experiments - Contract NAS8-28732, Massachusetts Institute of Technology Cambridge, Massachusetts, December 1973.

6. Monroe, R. E. and Pattee, H. E.; Characterization of Exothermic Brazing Comments - Skylab Experiment M552 - Contract NAS8-28725 , Battelle Columbus Laboratories, Columbus, Ohio, December 4, 1973.

7. Williams, J. R.; 90-Day Report - Skylab Experiment M552, NASA - George C. Marshall Space Flight Center, Huntsville, Alabama, October 1973.

8. Visual Observation of M552 Skylab Specimens and Hardware During NDT at MSFC, NASA-George C. Marshall Space Flight Center, Huntsville, Alabama, July 17, 1973.

9. Hansen, M., The Constitution of Binary Alloys, McGraw-Hill, New York, 1958, pp. 36-37.

10. Monroe, R.E., Report on Skylab M552 Samples, Battelle Memorial Institute, Columbus, Ohio, September 21, 1973.

11. Guertler, W. and Bergmann, A., Study of the Ternary Ag-Cu-Ni, Zeitschrifte fur Metallkunde, 25, 53 (1933).

12. Metals Handbook, 8, 380 (1973).

13. Backerud, L. and Liljenvall, L. M., The Solidification Characteristics of 7 Constitutionally Different Types of Binary Copper Alloys, INCRA Project 165, Swedish Institute for Metal Research, Stockholm, 1971.

TABLE I. M552 GROUND CHARACTERIZATION/FLIGHT SAMPLE ALLOCATION

Exotherm Heaters		Application	Braze At	Tube Position	Type Material	Isotope Tracer	Thermal Profile	Gap Dimension	Identification #
1	EXOTHERM MATERIAL Jan & June - 71	Astronaut Training Stainless	MSC		347			.002	AT 5
2			MSC	Horz	347			.002	AT 6
3			MSC	(All)	347			.002	AT 7
4			MSC		347			.002	AT 8
5		Metallurgical Characterization Stainless	MSFC		304L		X	.005	MCS 1
6			MSFC		304L		X	.005	MCS 2
7			MSFC	Horz	304L			.005	MCS 3
8			MSFC	(All)	304L			.020	MCS 4
9			MSFC		304L			.020	MCS 5
10			MSFC		304L			.020	MCS 6
11		Metallurgical Characterization Stainless	MSFC	Horz	Ni	X @ 12:00	X	.010	MCN 1
12			MSFC	Horz	Ni	X @ 3:00	X	.010	MCN 2
13			MSFC	Horz	Ni	X @ 6:00		.010	MCN 3
14			MSFC	Vert	Ni	X @ Bot		.000 - .030	MCN 4
15			MSFC	Vert	Ni	X @ Bot		.000 - .030	MCN 5
16			MSFC	Vert	Ni	X @ Bot		.000 - .030	MCN 6
17		Isotope Mapping	MSFC	Horz	Ni	X @ 3:00		.010	IMN 1
18			MSFC	Vert	Ni	X @ Bot		.000 - .030	IMN 2
19		Thermal Flow Data	MIT	Horz	347		X	.002	TF 1
20			MIT	(All)	347		X	.002	TF 2
21			MIT		347		X	.002	TF 3
1	EXOTHERM MATERIAL Dec - 72	Skylab Flight Samples	SKYLAB		304L			.005	SLS 1
2			SKYLAB		Ni	X		.010	SLN 2
3			SKYLAB	N.A.	304L			.020	SLS 3
4			SKYLAB		Ni	X		.000 - .030	SLN 4
5		Skylab Backup Samples	TO BE DETER-MINED		304L			.005	SBS 1
6					Ni	X		.010	SBN 2
7				N.A.	304L			.020	SBS 3
8					Ni	X		.000 - .030	SBN 4

N.A. - Not Applicable

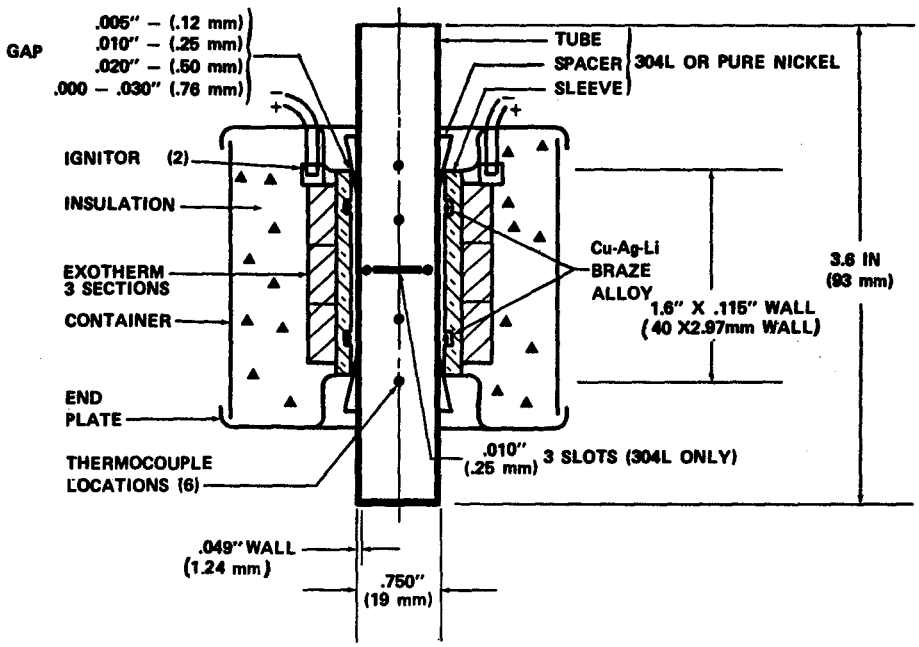

FIG. 1 CROSS SECTION - TUBE AND SLEEVE ASSEMBLY IN BRAZING CONTAINER

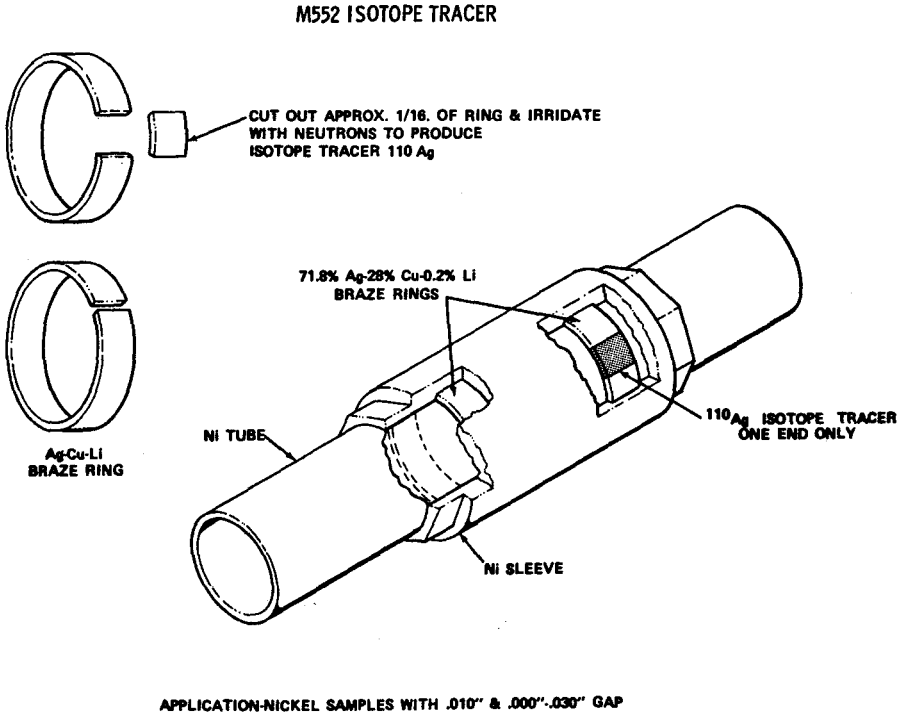

FIG. 2 ISOTOPE LOCATION - NICKEL SAMPLES

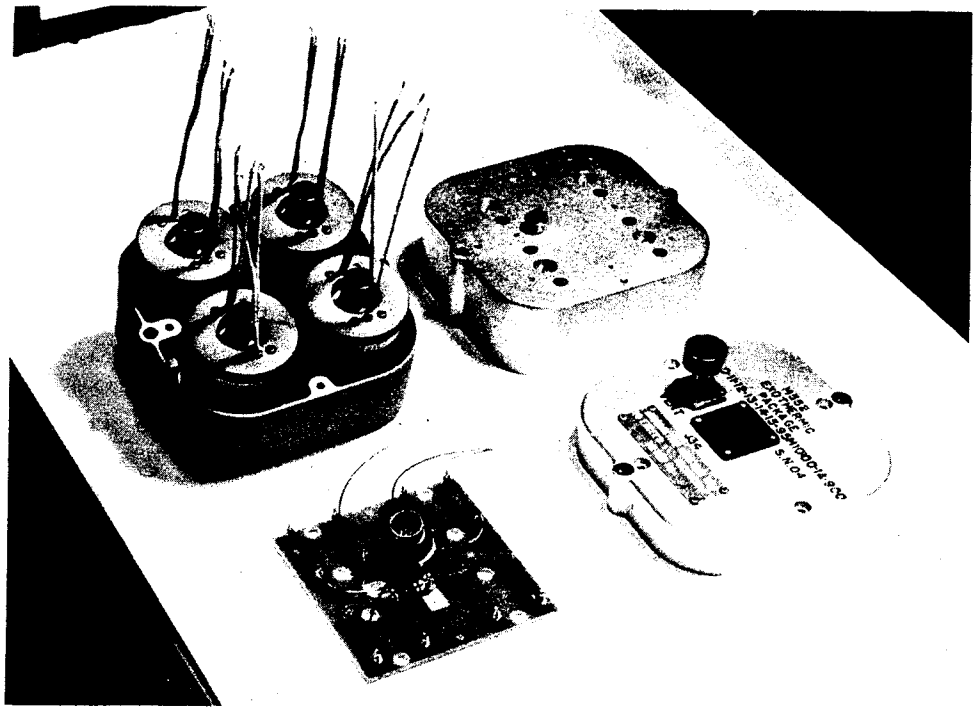

FIG. 3 HOUSING ASSEMBLY AND CONTENTS

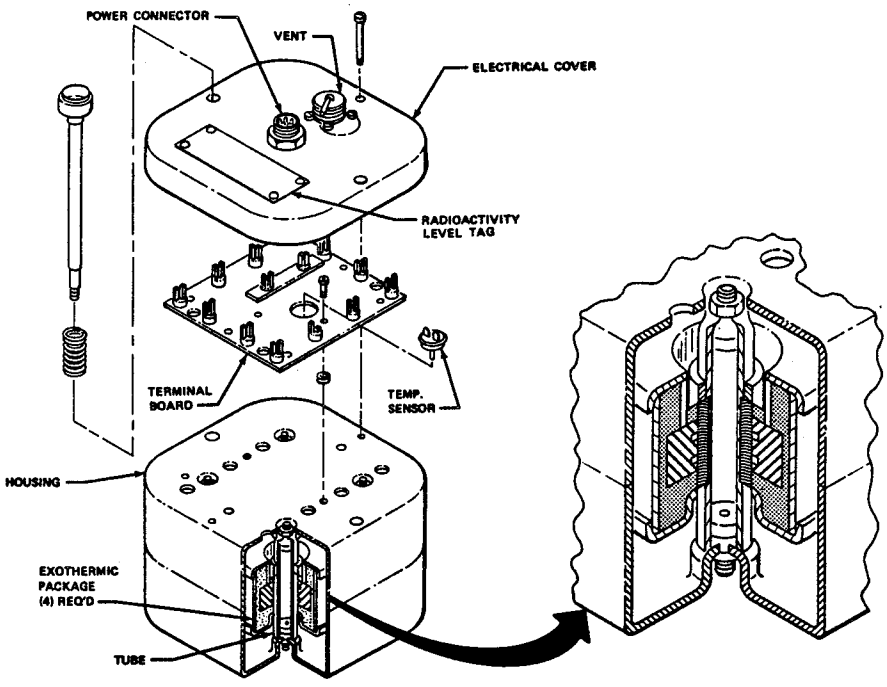

FIG. 4 M552 EXOTHERMIC PACKAGE AT ASSEMBLY

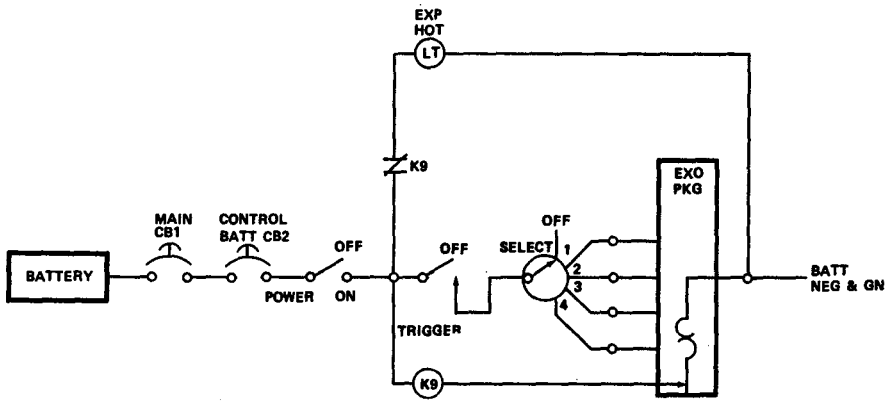

FIG. 5 SCHEMATIC OF M512 FACILITY ELECTRICAL CIRCUITS USED IN THE EXOTHERMIC BRAZING EXPERIMENT

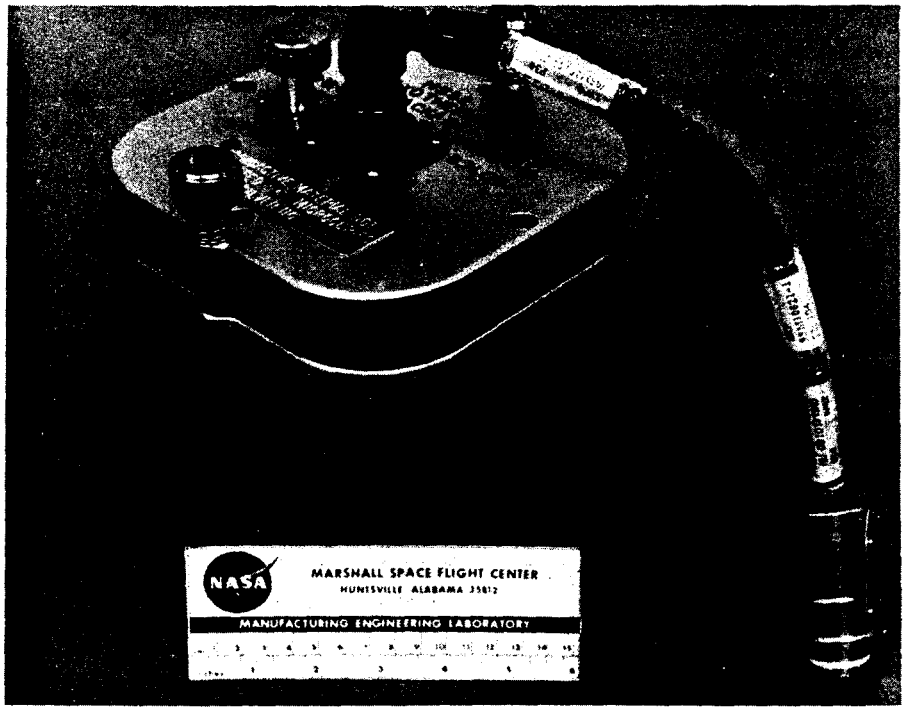

FIG. 6 M552 EXOTHERMIC PACKAGE AND ELECTRICAL POWER CABLE

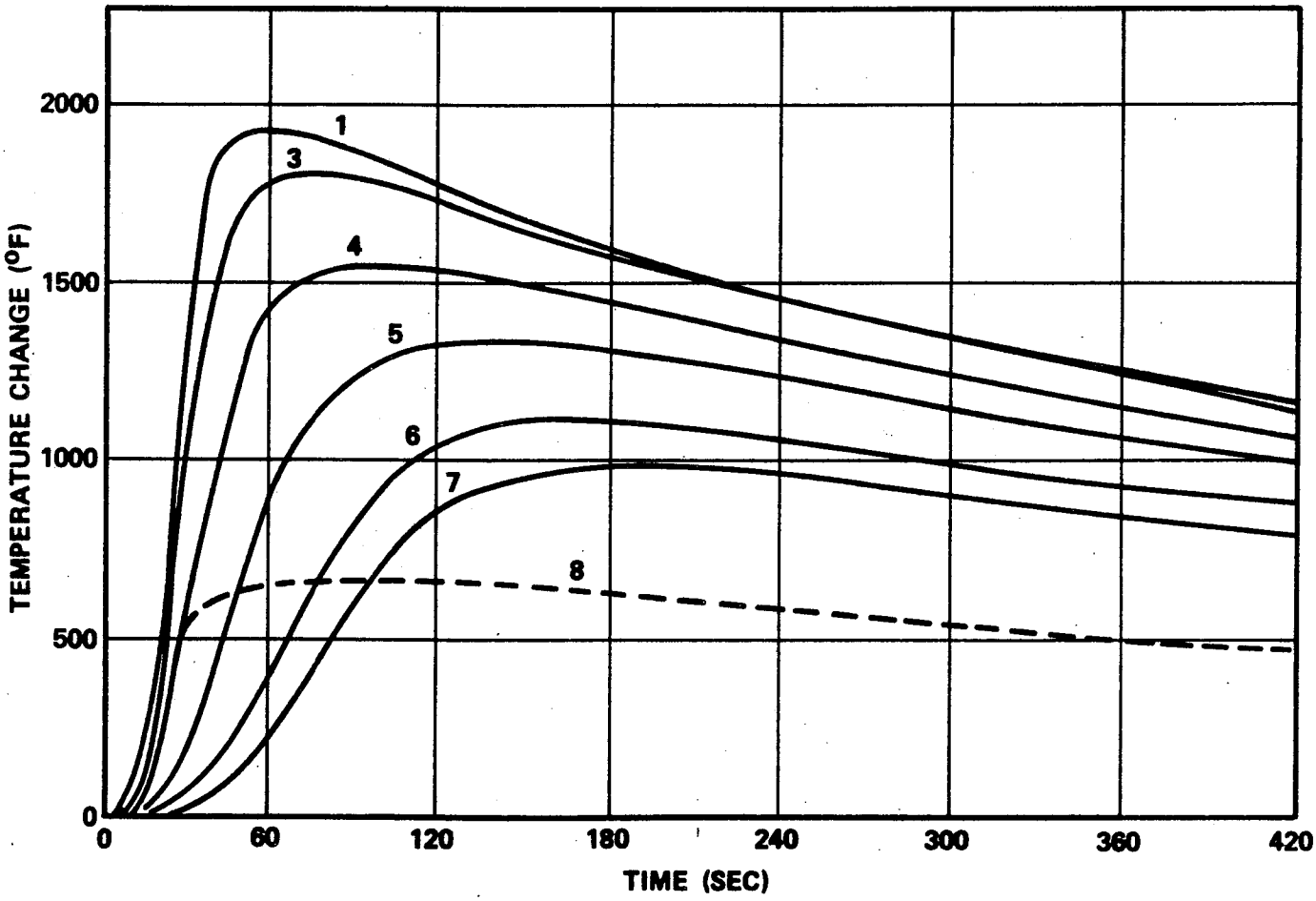

FIG. 7 TEMPERATURE PROFILE CURVES OF EXOTHERMIC HEATING OF TUBE

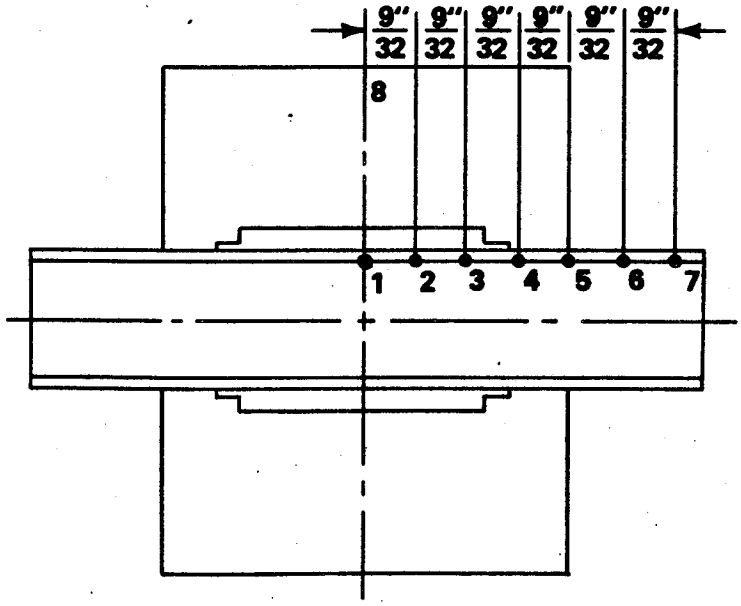

FIG. 8 THERMOCOUPLE LOCATIONS FOR TEST GENERATING CURVES IN FIGURE 7

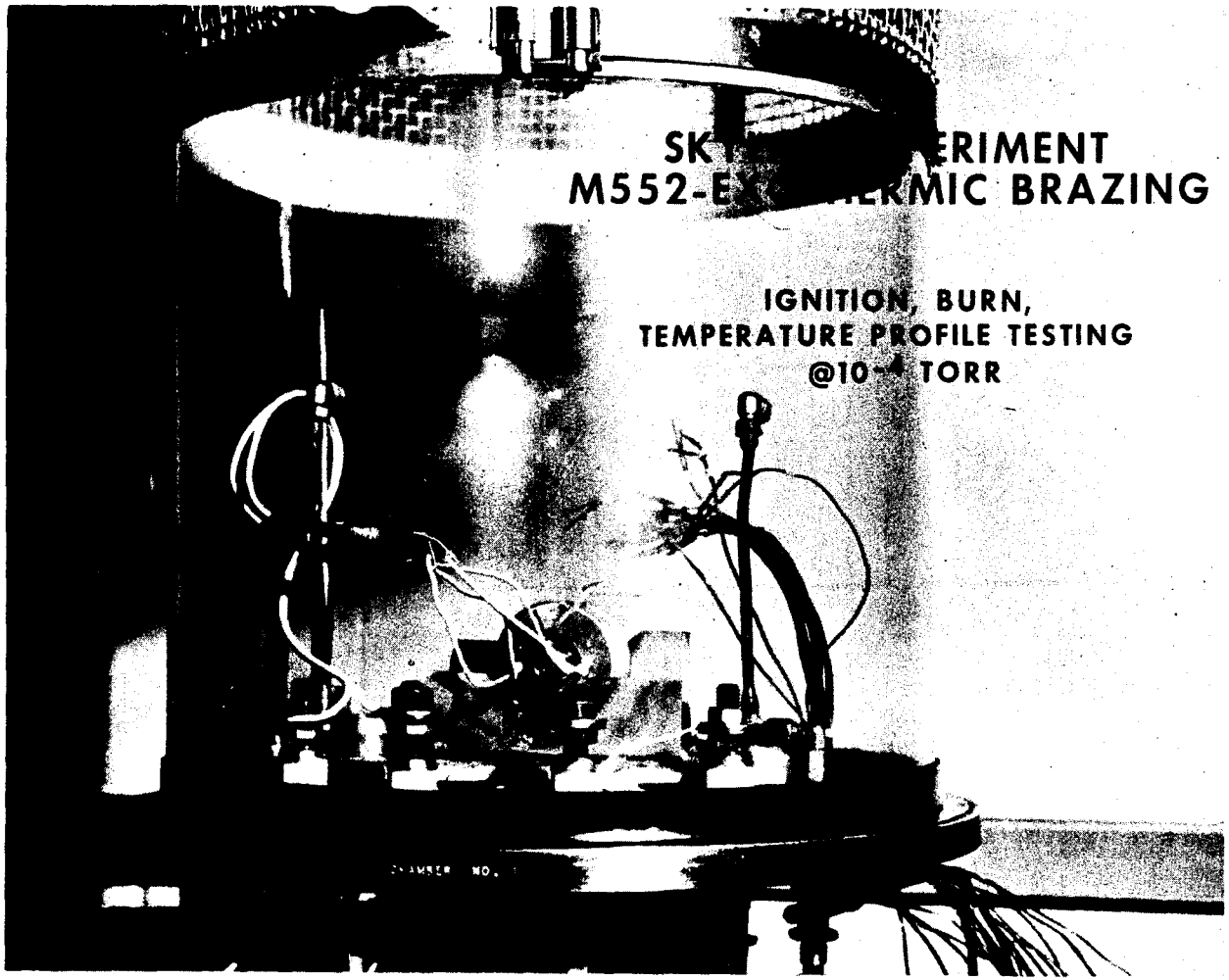

FIG. 9 IGNITION, BURN, TEMPERATURE PROFILE TESTING @ 10^{-4} TORR

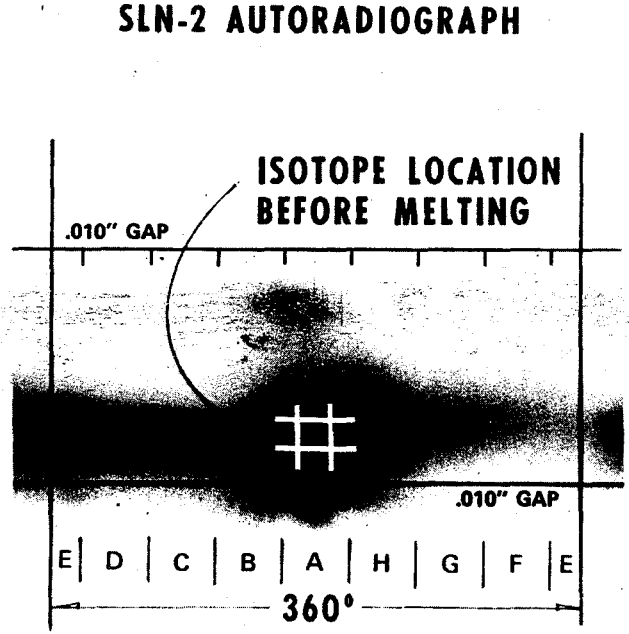

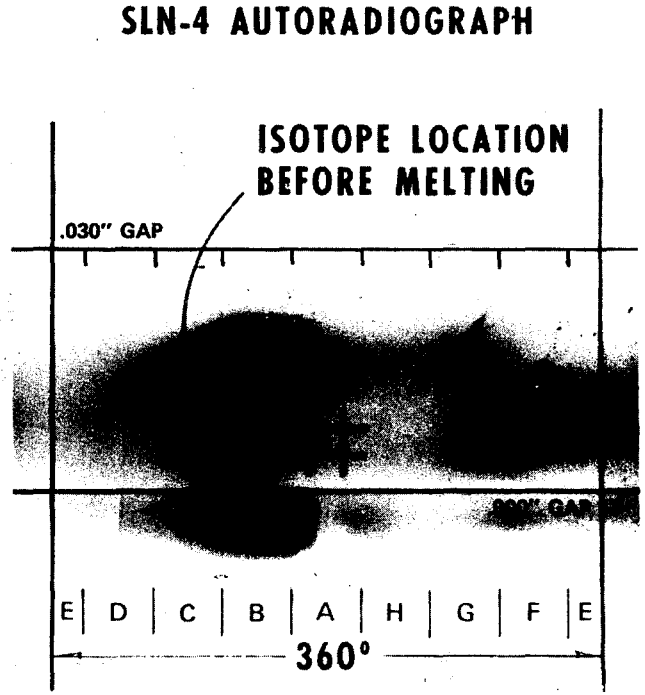

AUTO RADIOGRAPH OF 110 SILVER ISOTOPE AFTER MELTING, MOVEMENT VIA CAPILLARY FLOW & RESOLIDIFICATION IN PURE NICKEL SPECIMENS.

FIG. 10 AUTORADIOGRAPH OF SKYLAB SPECIMEN SLN-2

FIG. 11 AUTORADIOGRAPH OF SKYLAB SPECIMEN SLN-4

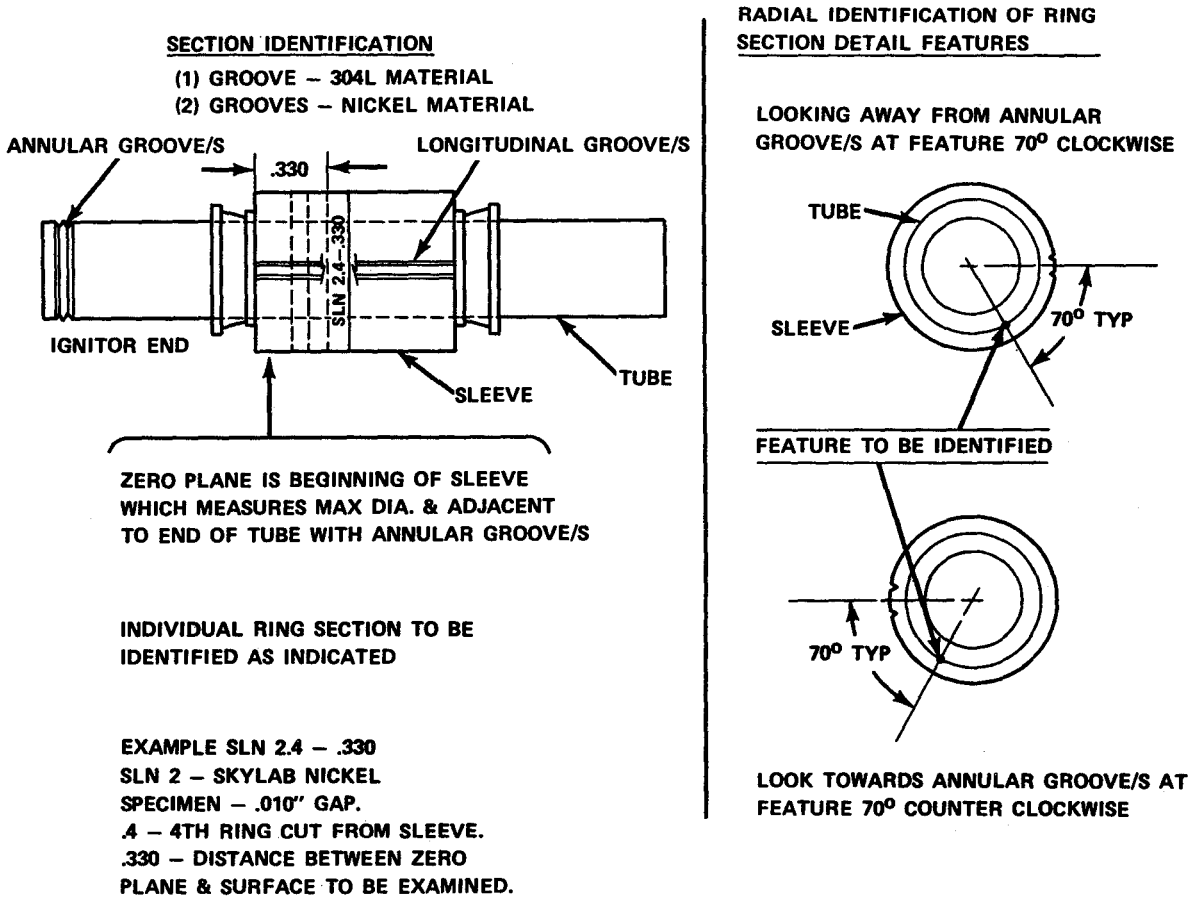

FIG. 12 M552 - IDENTIFICATION SECTIONING PLAN

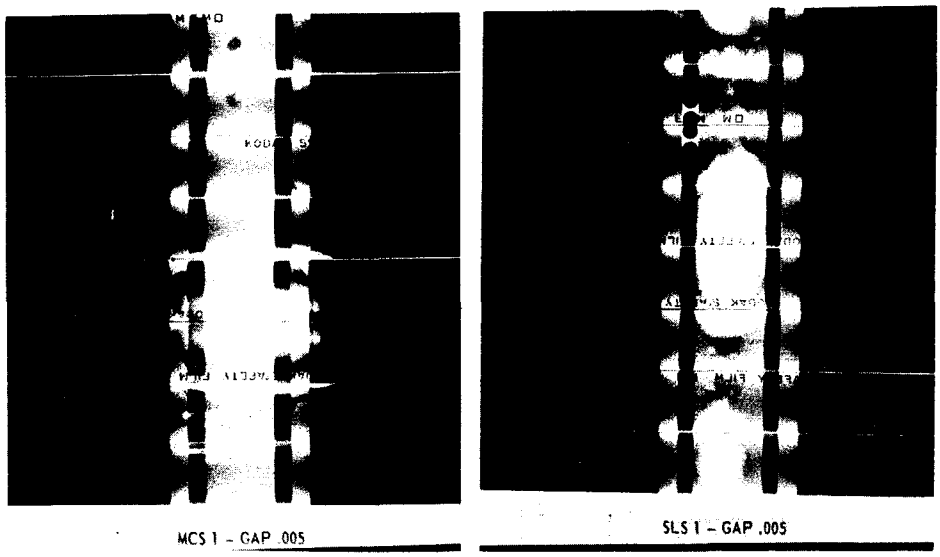

FIG. 13 MONTAGE RADIOGRAPH - SLS-1

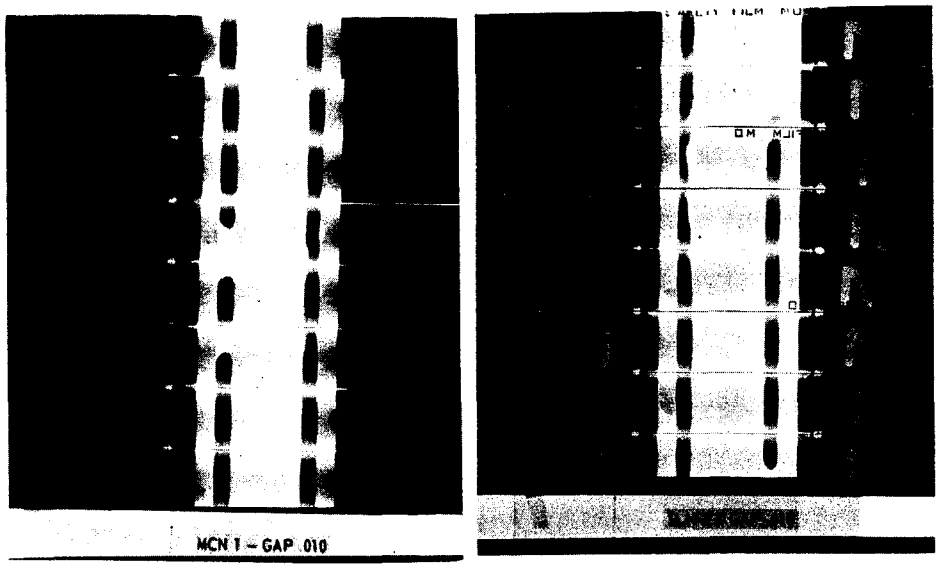

FIG. 14 MONTAGE RADIOGRAPH - SLN-2

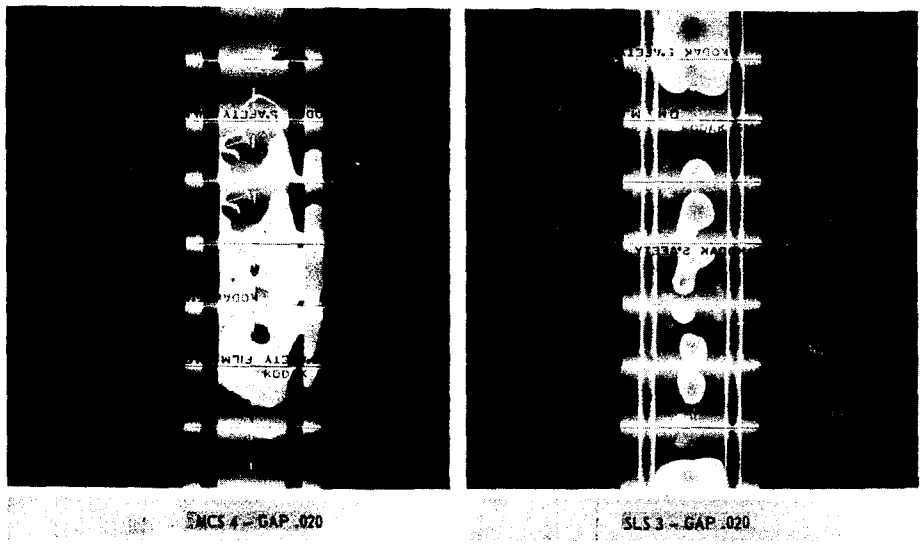

FIG. 15 MONTAGE RADIOGRAPH - SLS-3

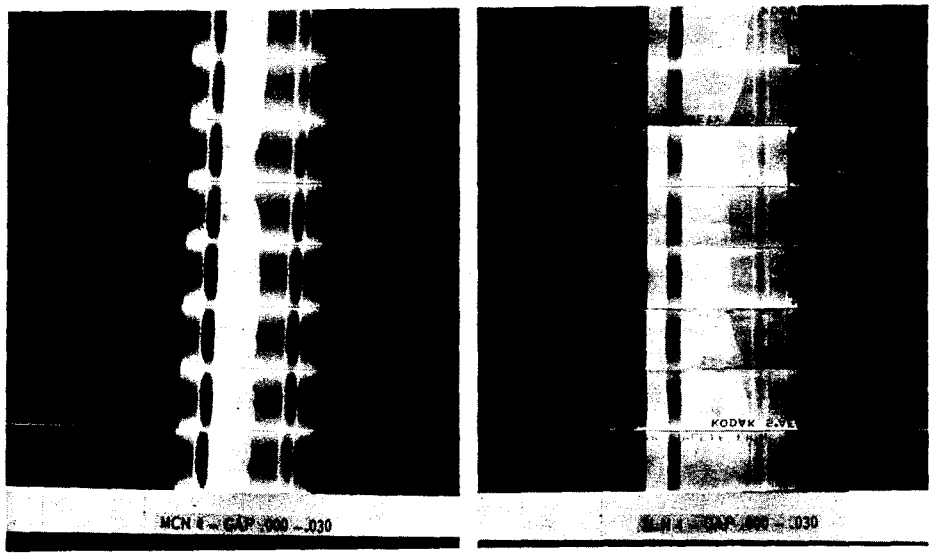

FIG. 16 MONTAGE RADIOGRAPH - SLN-4

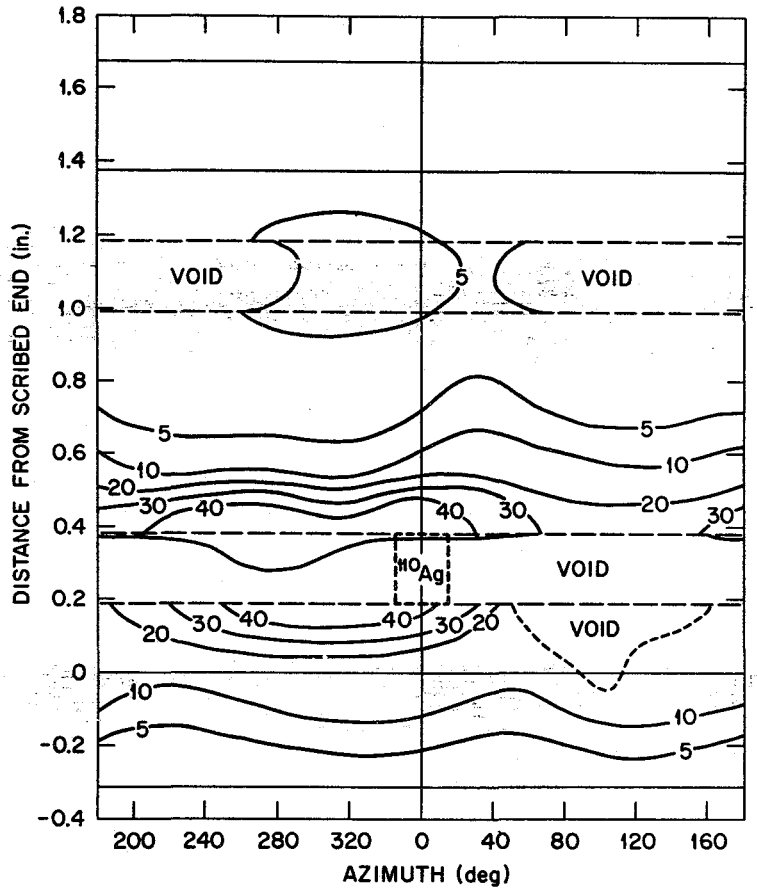

FIG. 17 ISOTOPE INTENSITY MAP - SLN-2

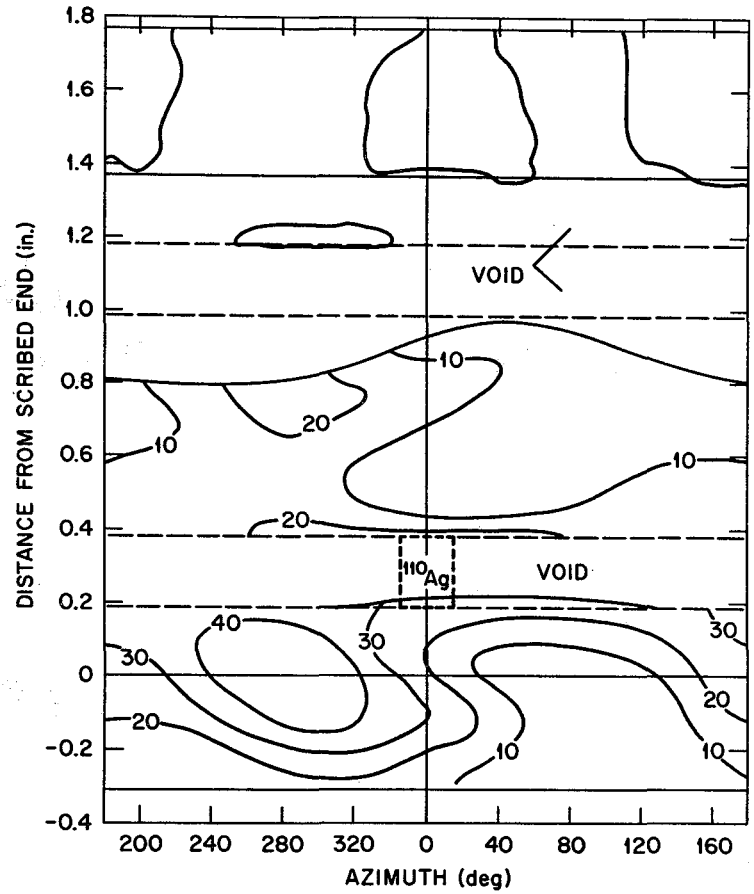

FIG. 18 ISOTOPE INTENSITY MAP - SLN-4

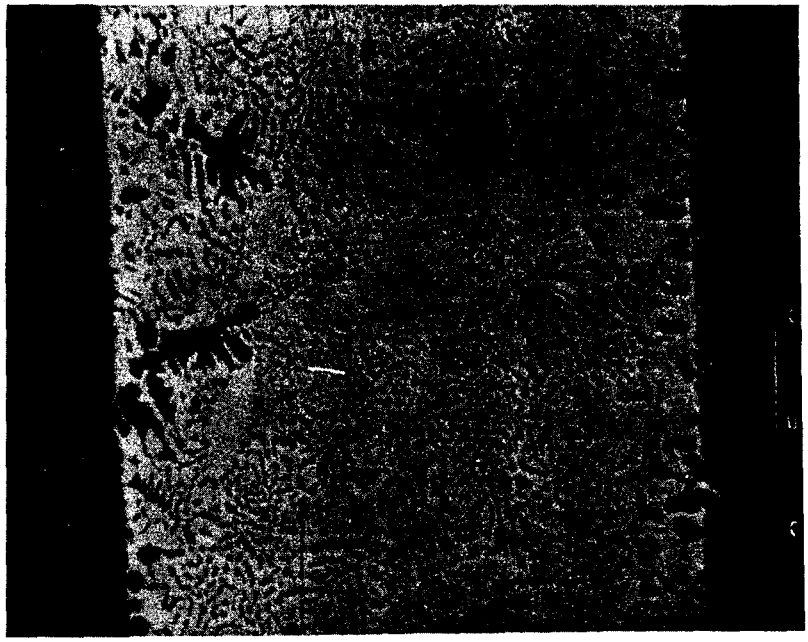

FIG. 19 SCANNING ELECTRON MICROGRAPH OF SLN-4-20mm - 120° SHOWING THE TWO KINDS OF PRIMARY PHASES. (250X)

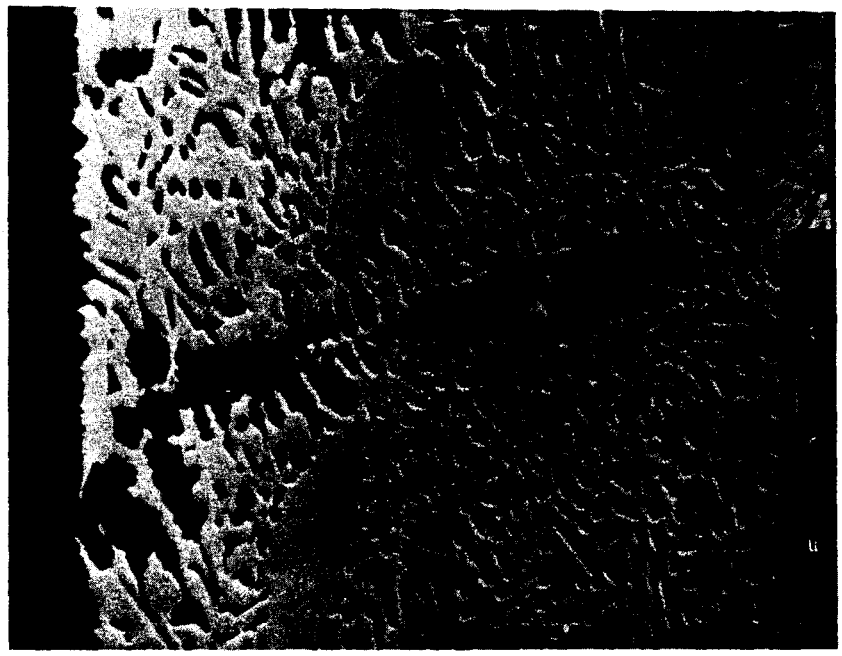

FIG. 20 CLOSE-UP OF THE SAME REGION SHOWN IN FIGURE 19. NOTICE THE DARK COPPER PHASE EXTENDING FROM THE NICKEL SURFACE WITH THREE LIGHT SILVER PHASE REGIONS AT ITS TIP. (500X)

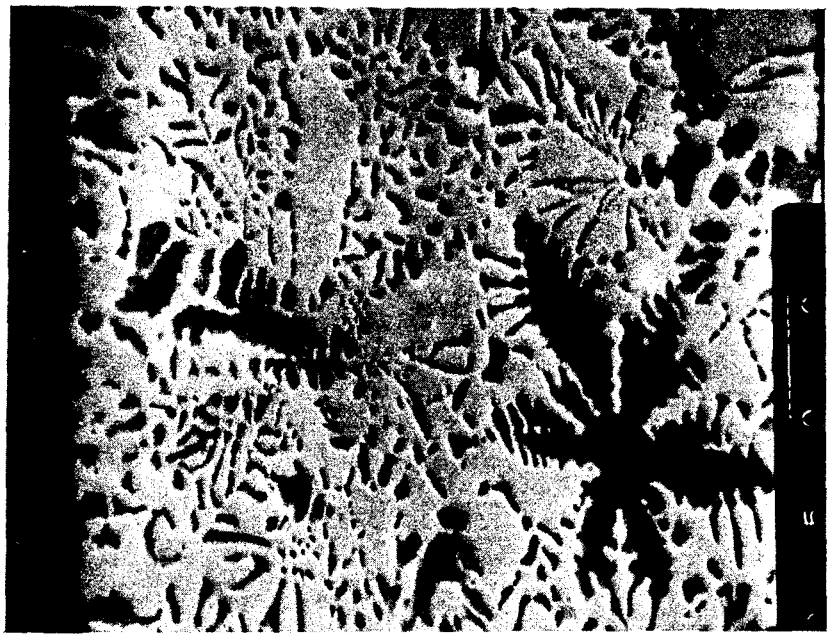

FIG. 21 SCANNING ELECTRON MICROGRAPH OF SLN 4-21mm -120° SHOWING SIMILAR STRUCTURE TO FIGURES 19 AND 20. (500X)

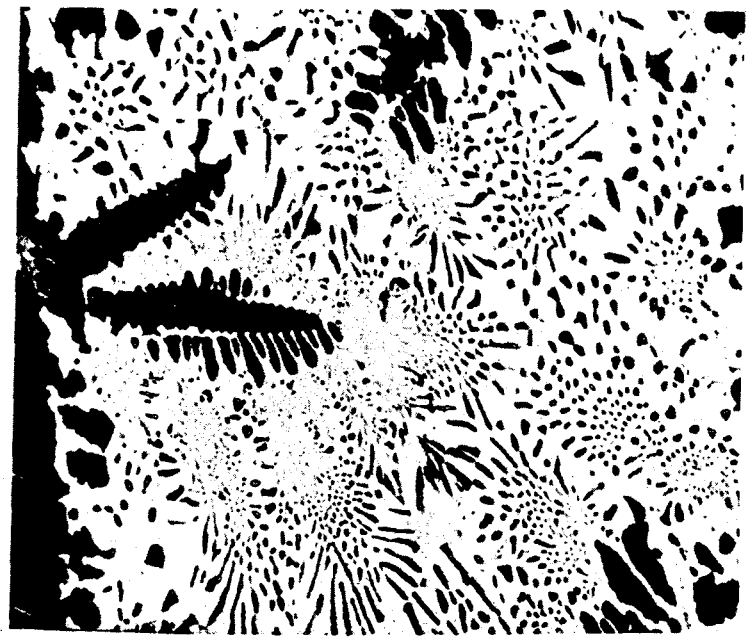

FIG. 22 SCANNING ELECTRON MICROGRAPH OF MCN 6-8mm - 90° SHOWING A TYPICAL COPPER-RICH DENDRITE AND COPPER-RICH REACTION LAYER ADJACENT TO THE PURE NICKEL AT THE FAR LEFT. (500X)

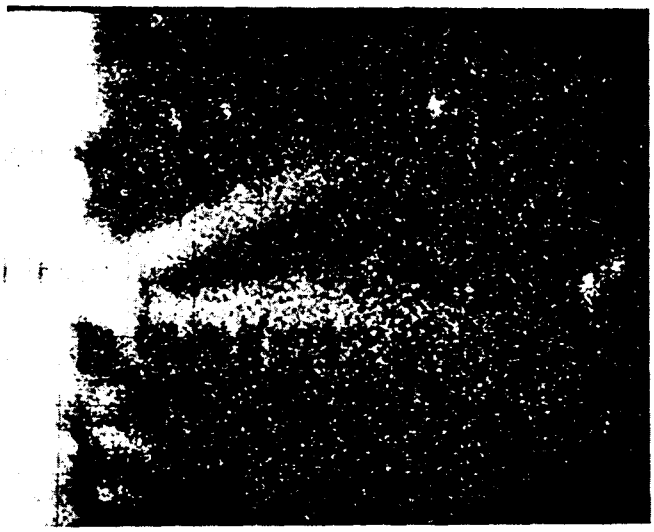

FIG. 23 NICKEL K_α X-RAY SCAN OF THE SAME REGION AS FIGURE 22. THE LIGHT AREAS SHOW THE HIGHEST NICKEL CONCENTRATIONS. (500X)

FIG. 24 COPPER K_α X-RAY SCAN OF THE SAME REGION AS FIGURE 22. (500X)

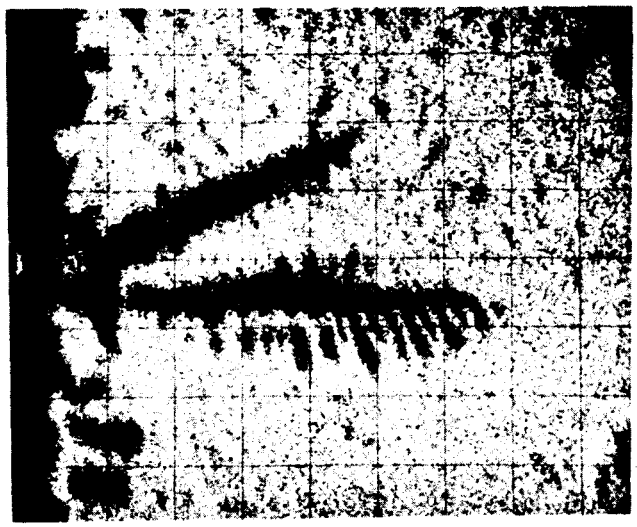

FIG. 25 SILVER Lα X-RAY SCAN OF THE SAME REGION AS FIGURE 22. (500X)

FIG. 26 SCANNING ELECTRON MICROGRAPH OF SLN 4-5mm - 290° WITH A LARGE DENDRITE. (250X)

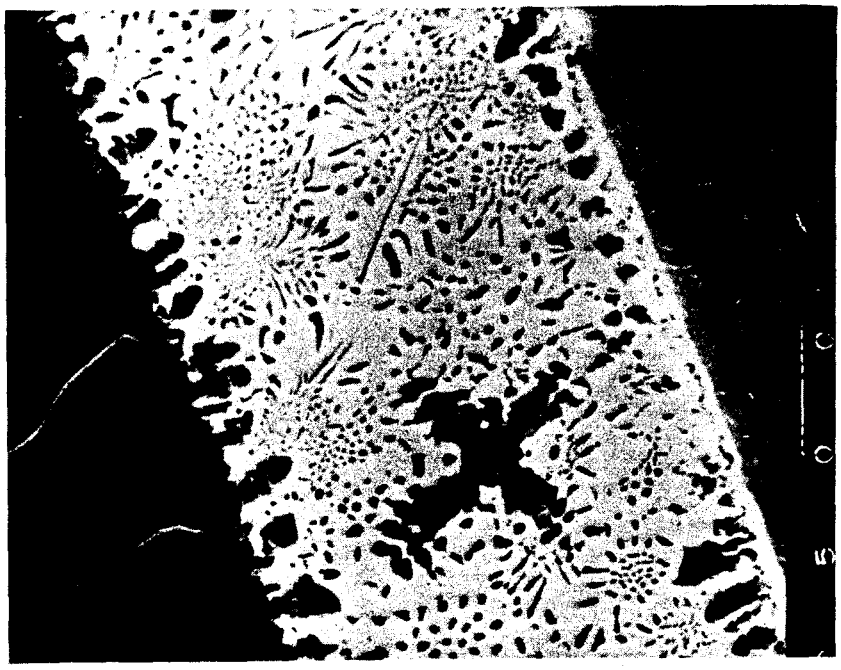

FIG. 27 SCANNING ELECTRON MICROGRAPH OF SLN 4-18mm - 90° ILLUSTRATING THE NORMAL STRUCTURE. (500X)

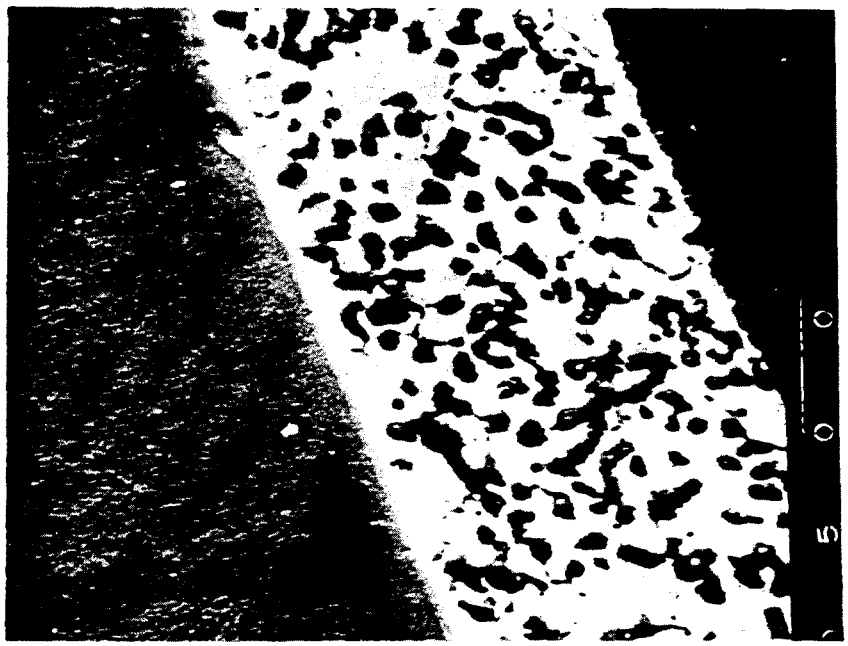

FIG. 28 SCANNING ELECTRON MICROGRAPH OF SLN 4-18mm - 65° ILLUSTRATING THE ABNORMAL STRUCTURE. (500X)

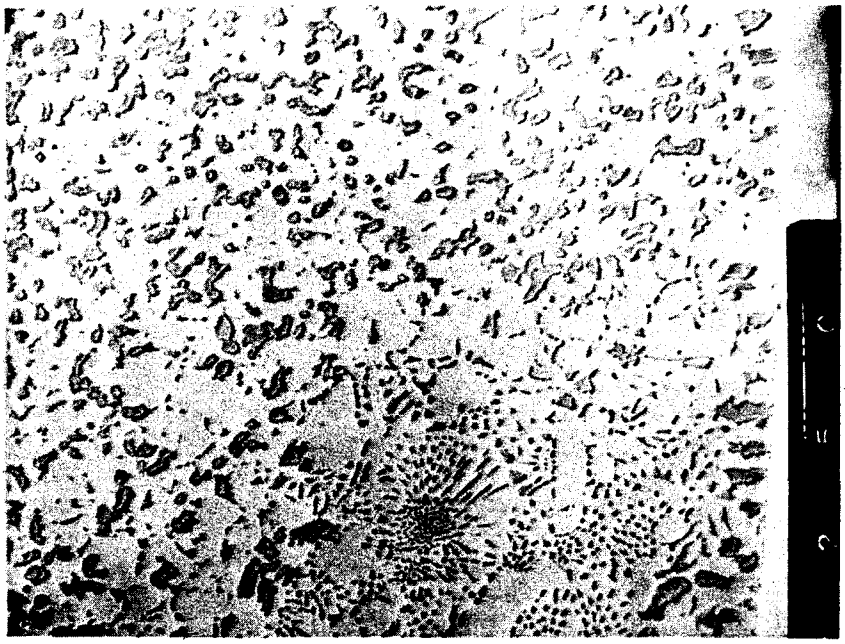

FIG. 29 SCANNING ELECTRON MICROGRAPH OF SLN 4-33mm - 220° ILLUSTRATING THE MIXTURE OF NORMAL AND ABNORMAL STRUCTURE IN THE RING-GROOVE FARTHEST FROM THE ZERO PLANE. (250X)

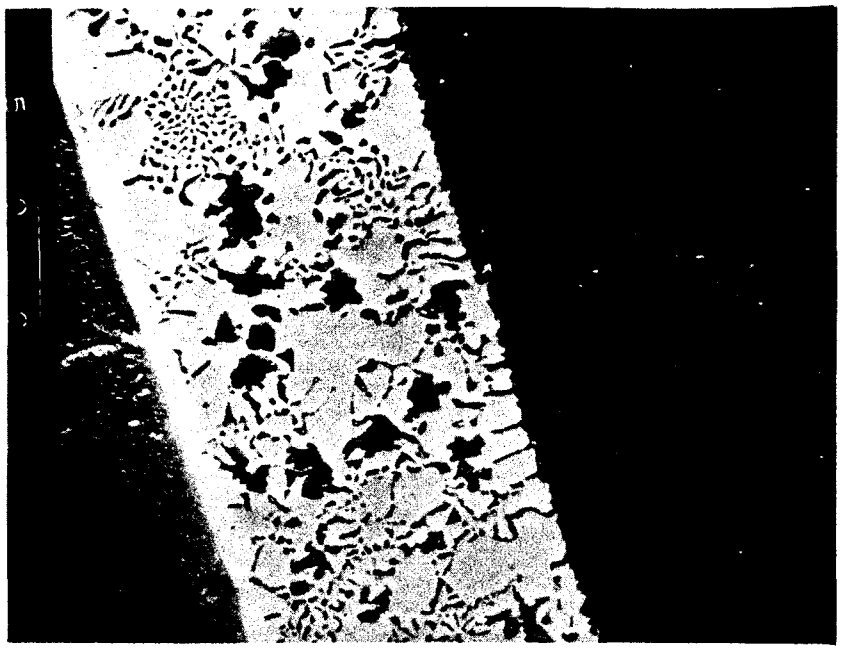

FIG. 30 SCANNING ELECTRON MICROGRAPH OF SLN 4-18mm - 75° ILLUSTRATING THE MIXED STRUCTURE. (500X)

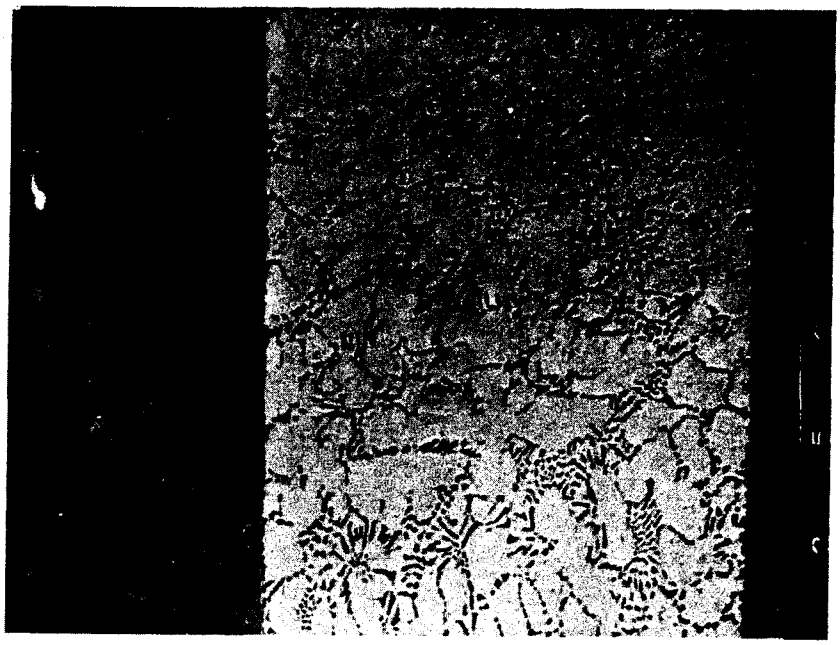

FIG. 31 SCANNING ELECTRON MICROGRAPH OF SLS 3-13mm - 150° SHOWING THE PRIMARY SILVER-RICH DENDRITES (LARGE WHITE AREAS) WHICH WERE NOT OBSERVED ON GROUND CHARACTERIZATIONS. (250X)

FIG. 32 SCANNING ELECTRON MICROGRAPH OF SLS 3-17mm - 5° SHOWING A MORE EXTREME CASE OF THE PRIMARY SILVER-RICH DENDRITES SEEN IN FIGURE 31. (500X).

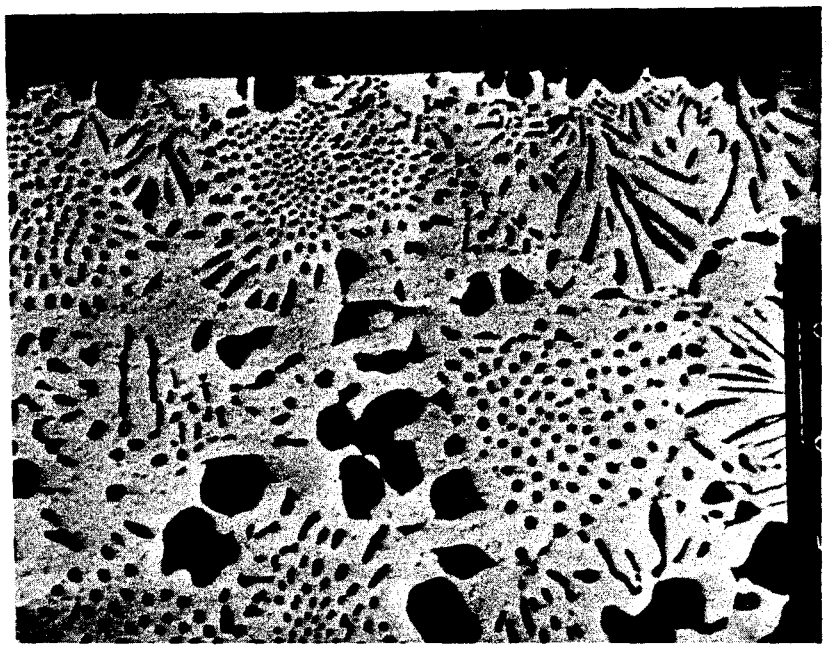

FIG. 33 SCANNING ELECTRON MICROGRAPH OF SLS 3-28mm - 5° SHOWING DENDRITES PRESENT IN THE RING-GROOVE ALONG WITH THE COMPLETE ABSENCE OF THE PRIMARY SILVER PHASE SHOWN IN FIGURES 31 AND 32. (250X)

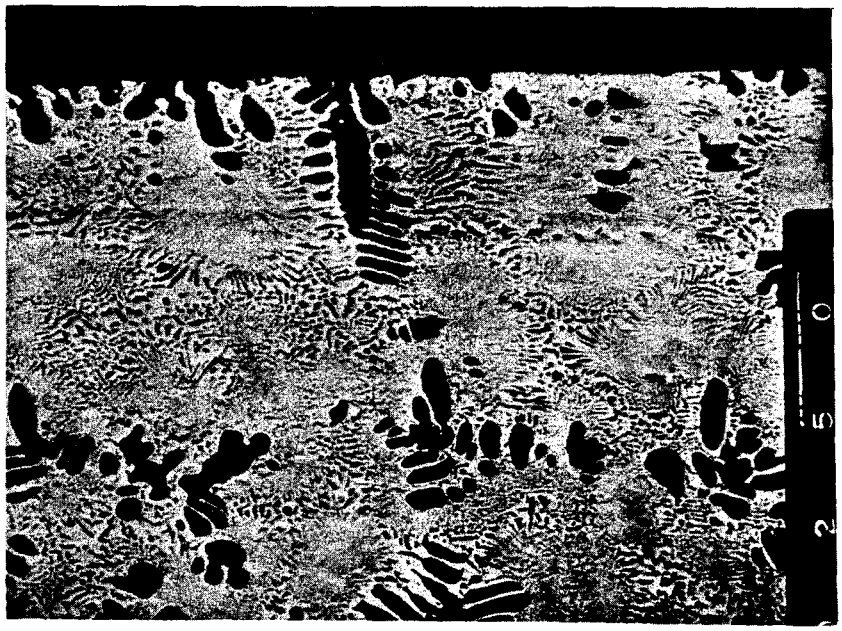

FIG. 34 SCANNING ELECTRON MICROGRAPH OF MCS 6-11.7mm - 260° SHOWING THE NORMAL EUTECTIC ADJACENT TO STAINLESS SURFACE (AT TOP). (500X)

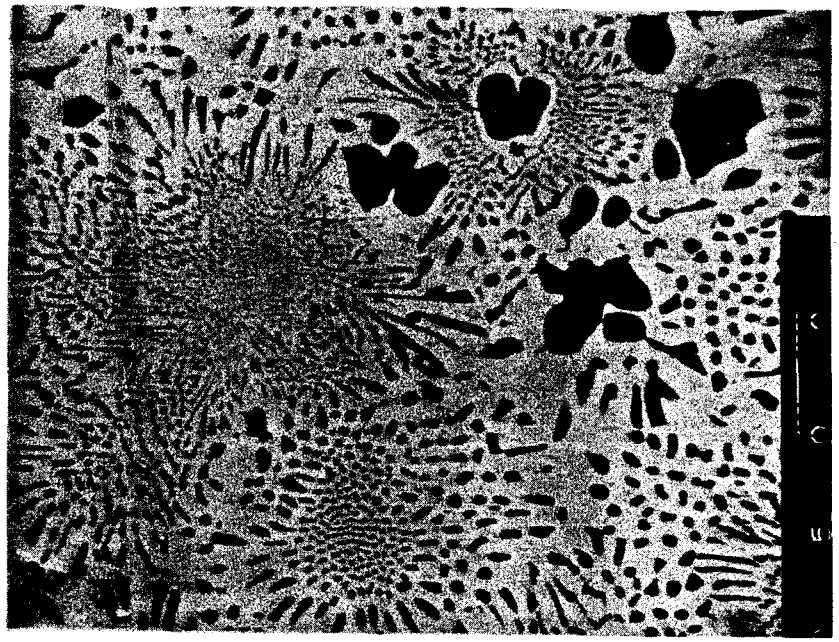

FIG. 35 SCANNING ELECTRON MICROGRAPH OF MCS 6-11.7mm - 280° SHOWING AGAIN THE GROUND CHARACTERIZATION MICROSTRUCTURE. (500X)

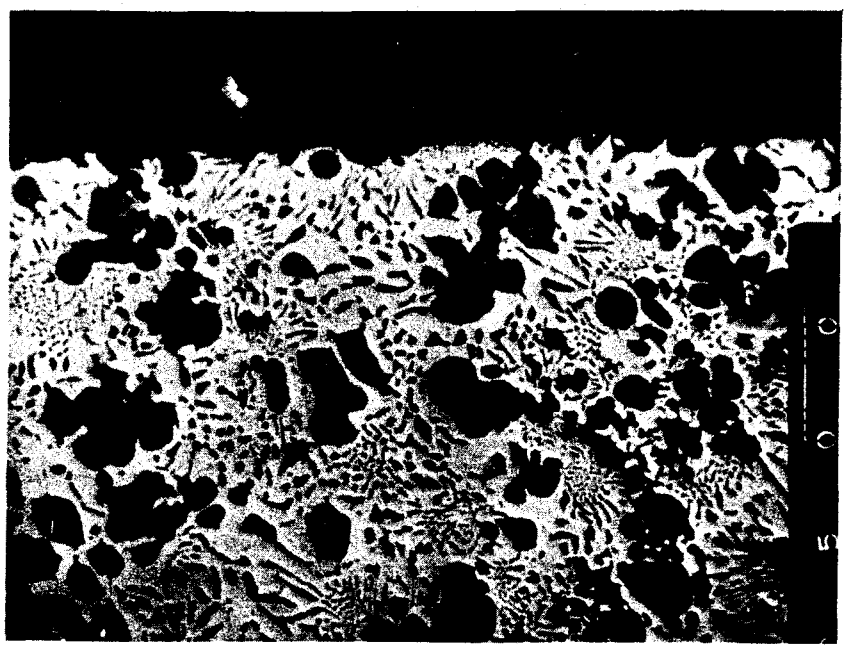

FIG. 36 SCANNING ELECTRON MICROGRAPH OF SLS 3-7mm - 315° SHOWING STAINLESS STEEL PARTICLES NEAR STAINLESS STEEL-BRAZE ALLOY INTERFACE. (500X)

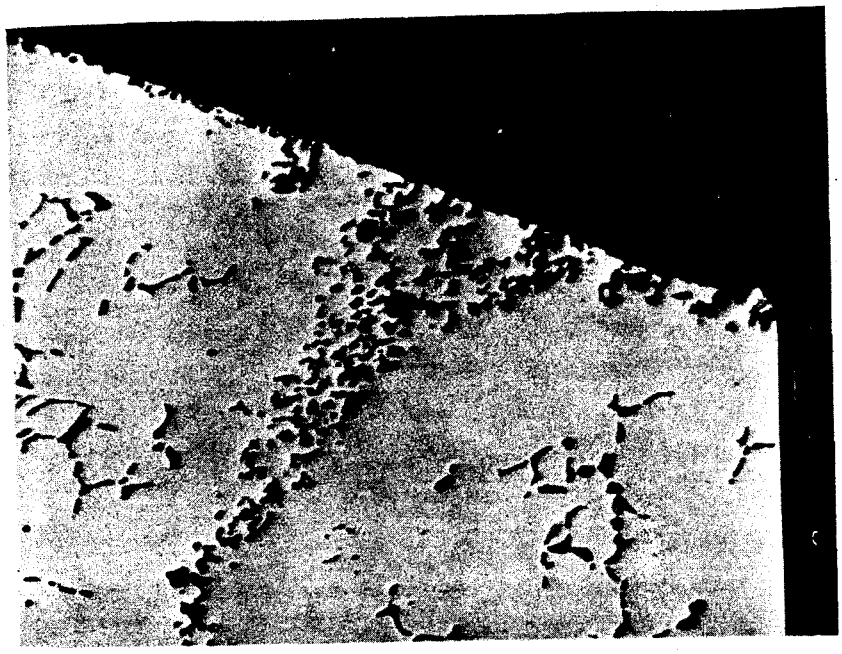

FIG. 37 SCANNING ELECTRON MICROGRAPH OF SLS 3-12mm -5° SHOWING STAINLESS PARTICLES IN BRAZE ALLOY. (500X)

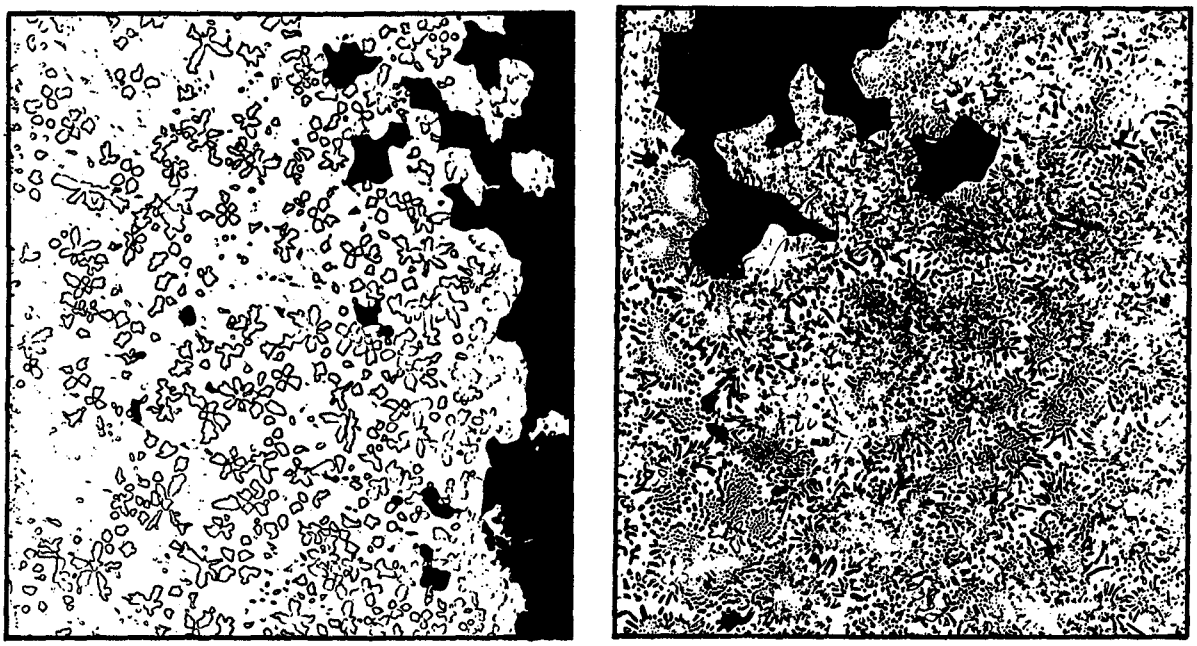

Skylab Ground

Microstructure Ring Groove 100X

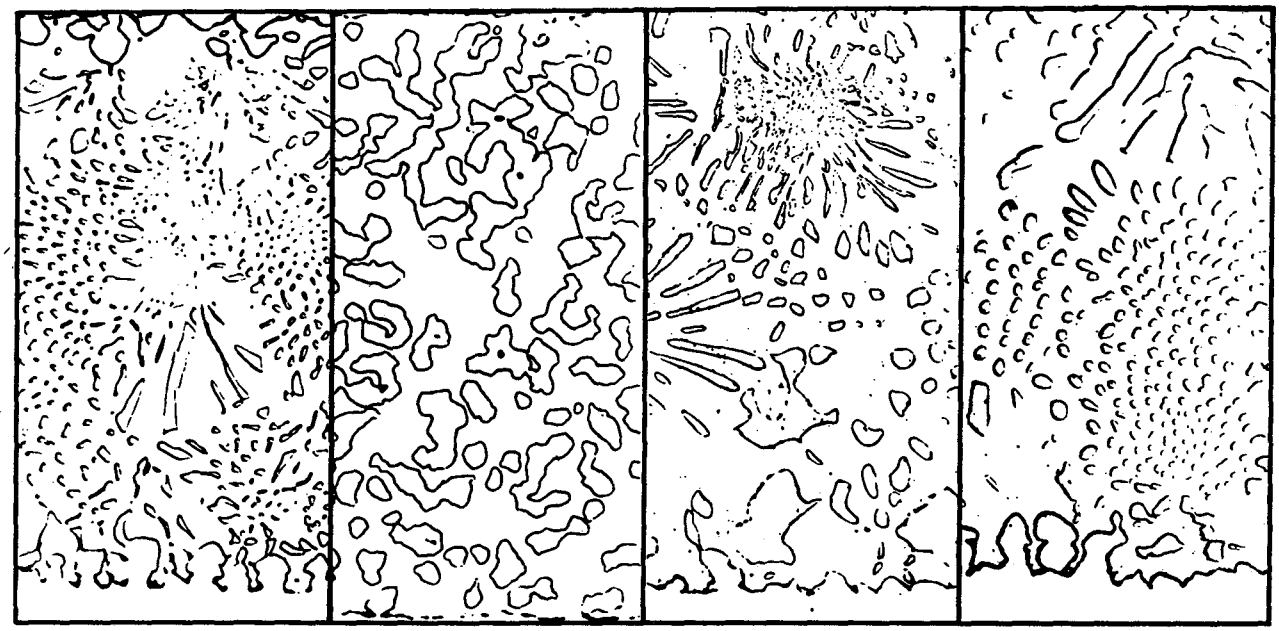

Skylab Ground

Microstructure in Braze Gap-500X

FIG. 38 COMPARISON OF MICROSTRUCTURES IN SKYLAB SPECIMEN SLN-2 AND GROUND BASED NICKEL BRAZE SPECIMENS.

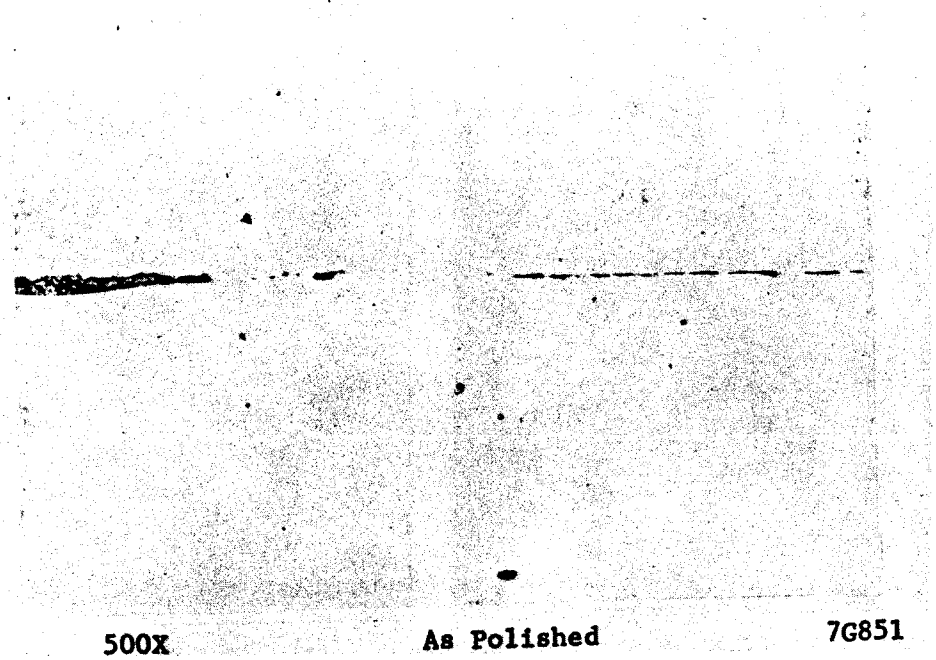

SOLID-STATE BOND AREA -
SECTION SLS-1.4 (14 mm and 0°)

FIG. 39 DIFFUSION BONDED AREA FORMED IN SKYLAB STAINLESS STEEL SPECIMEN SLS-1.

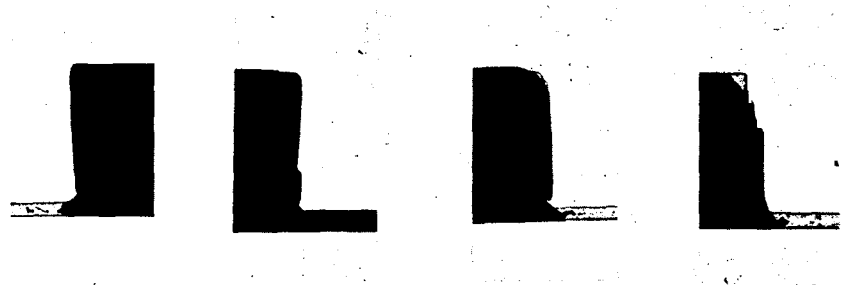

a. Ground Specimens

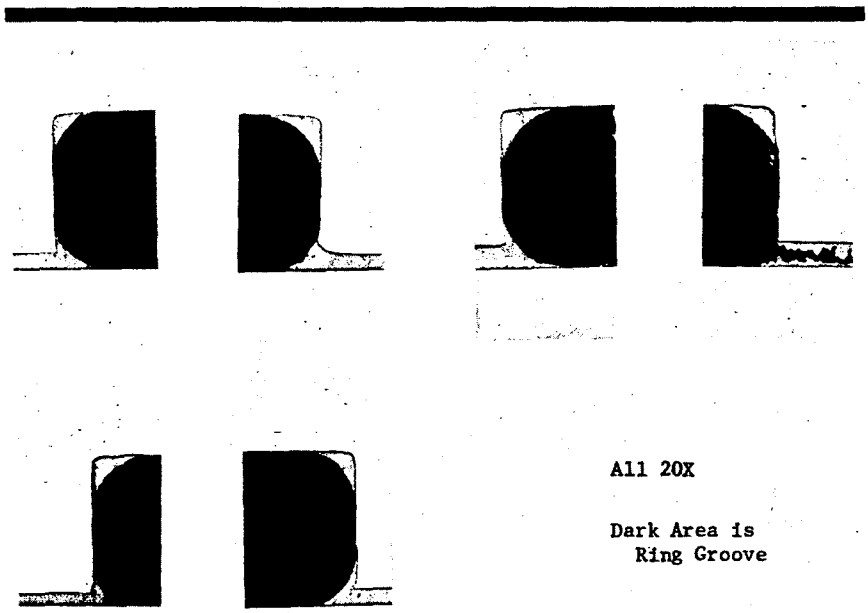

b. Skylab Specimens

FIG. 40 COMPARISON BETWEEN RETAINED FILLET OF 304L GROUND BASED FILLET AND SKYLAB SLS-1 SPECIMEN

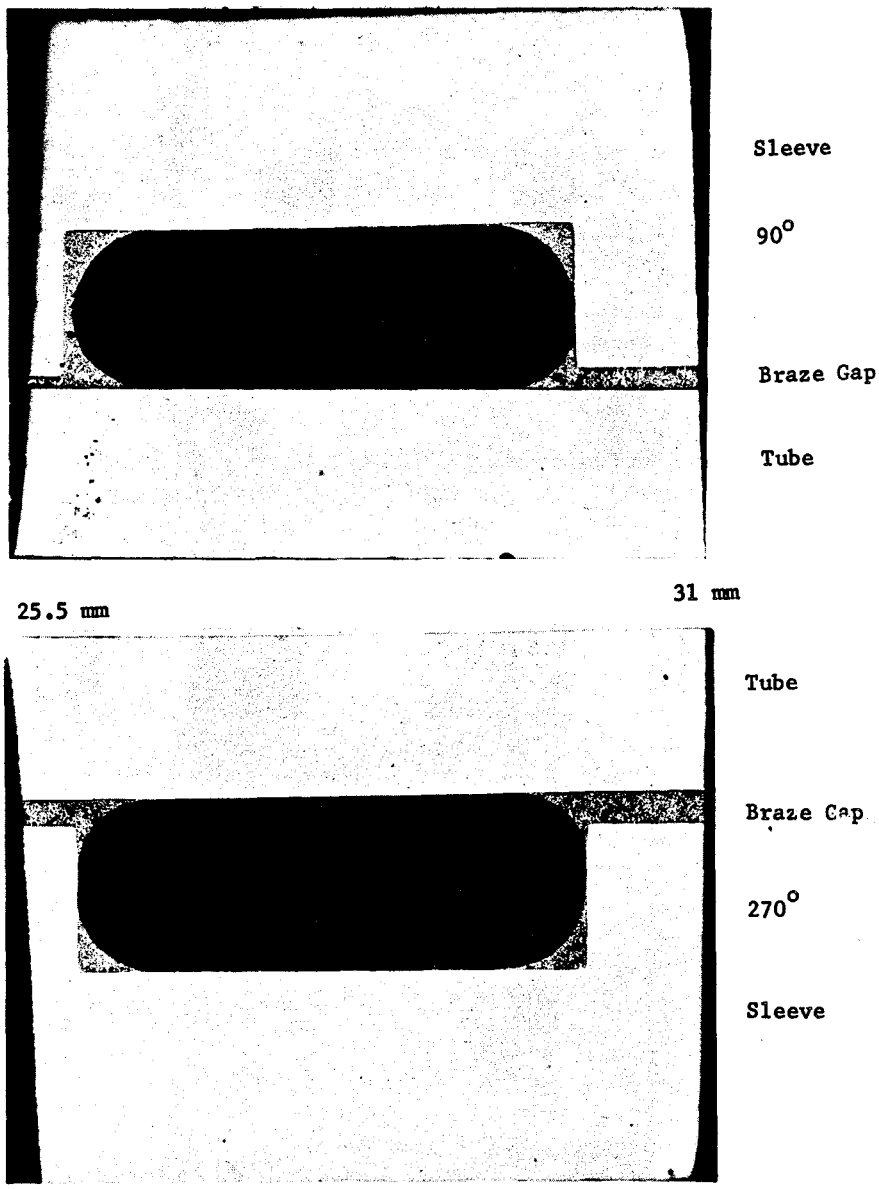

FIG. 41 CLASSIC EXAMPLE OF A BRAZE MATERIAL FILLET RETAINED IN RING GROOVE-SKYLAB SAMPLE SLN-2